AD-A121 444 ACOUSTIC TRANSMISSION BETWEEN COUPLED CAVITIES(U) 1/1
ADMIRALTY MARINE TECHNOLOGY ESTABLISHMENT TEDDINGTON
(ENGLAND) A J ROBINS JUL 82 AMTE(N)/R82002
UNCLASSIFIED DRIC-BR-85080 F/G 20/1 NL

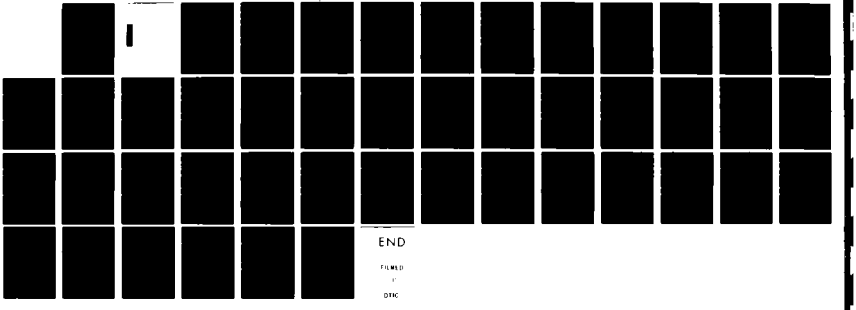

END

FILMED
DTIC

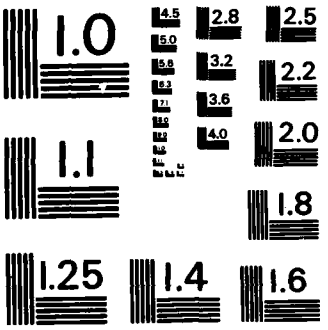

MICROCOPY RESOLUTION TEST CHART
NATIONAL BUREAU OF STANDARDS-1963-A

AMTE(N)R82002

ACOUSTIC TRANSMISSION BETWEEN COUPLED CAVITIES (U)

BY

A J ROBINS

Summary

As part of an investigation of flow induced cavity resonance, experimental studies have been carried out, both in air and water, on systems of coupled cavities (ie cavities connected by a common opening). The work was performed with the aim of examining the effects on sound transmission between cavities, of parameters such as wall flexibility, fluid viscosity and the size of opening connecting the cavities. Theoretical models have been developed to describe the acoustic behaviour of the cavity systems studied, and good agreement is obtained between theory and experiment. It is concluded that, for most practical applications, the effect of viscosity on sound transmission between resonating cavities is negligible. Flexibility of the boundaries is, however, a dominating factor whose effects are particularly noticeable when the fluid medium is water.

50 PAGES.
14 FIGURES.

AMTE (Teddington)
Queens Road
TEDDINGTON Middx TW11 OLN July 1982

INTRODUCTION

A number of experimental studies have recently been carried out at AMTE Teddington on the topic of flow induced cavity resonance (see, for example, Reference 1). In parallel with this work, interest has arisen in the acoustic behaviour of systems of coupled cavities since, in some cases of practical interest, resonance excited by an external flow may occur in a complex structure containing many interconnected chambers, rather than a single cavity. The aim of the study described in this report is to estimate the effects of various parameters, such as viscous damping and wall flexibility, on the acoustic transmission between coupled cavities. This has been accomplished by two separate experimental studies, with corresponding theoretical modelling. The first study, aimed at investigating the effect of viscous damping, was carried out in air. In this case the cavity walls can be regarded as acoustically rigid. The simple geometry of the system, which is described in detail in the following section, permits an exact solution of the reduced wave equation in the form of an eigenfunction expansion. This theoretical model is valid over a fairly wide range of frequencies. The second study was carried out with water as the fluid medium,using a more complicated system of cavities with non-rigid walls. Eigenfunction expansion techniques could not be used for the theoretical description of this system, so a much simpler model, valid only at low frequencies, was developed to describe its acoustic behaviour. The simplified approach may also be used to describe the behaviour of the rigid walled cavity system at low frequencies.

It is possible to analyse systems of coupled cavities using finite element methods, but this analysis can be very complex even for relatively simple systems. Fahmy [2] has used the finite element technique to study the behaviour of two cavities coupled via a common opening and has obtained good agreement with experimental results. However, his analysis is restricted to the case of acoustically hard walls, which is unrealistic in underwater applications. The approach adopted by Fahmy could be generalised to cope with non-rigid boundaries, but the computational effort required was felt not to be worthwhile for the purposes of the present study. The aim of the theoretical models described here is to quantify the relative importance of various parameters and to provide physical understanding of the observed experimental results. This can best be achieved with relatively simple mathematical models, even though their range of validity may be somewhat restricted in comparison with more sophisticated techniques. Details of both experimental and theoretical results are presented and discussed in the following pages.

2. RIGID WALLED CAVITY SYSTEM

(a) Experiment

The experiments described in this section were carried out in the anechoic chamber at AMTE Teddington. The rig is illustrated in Figure 1 below.

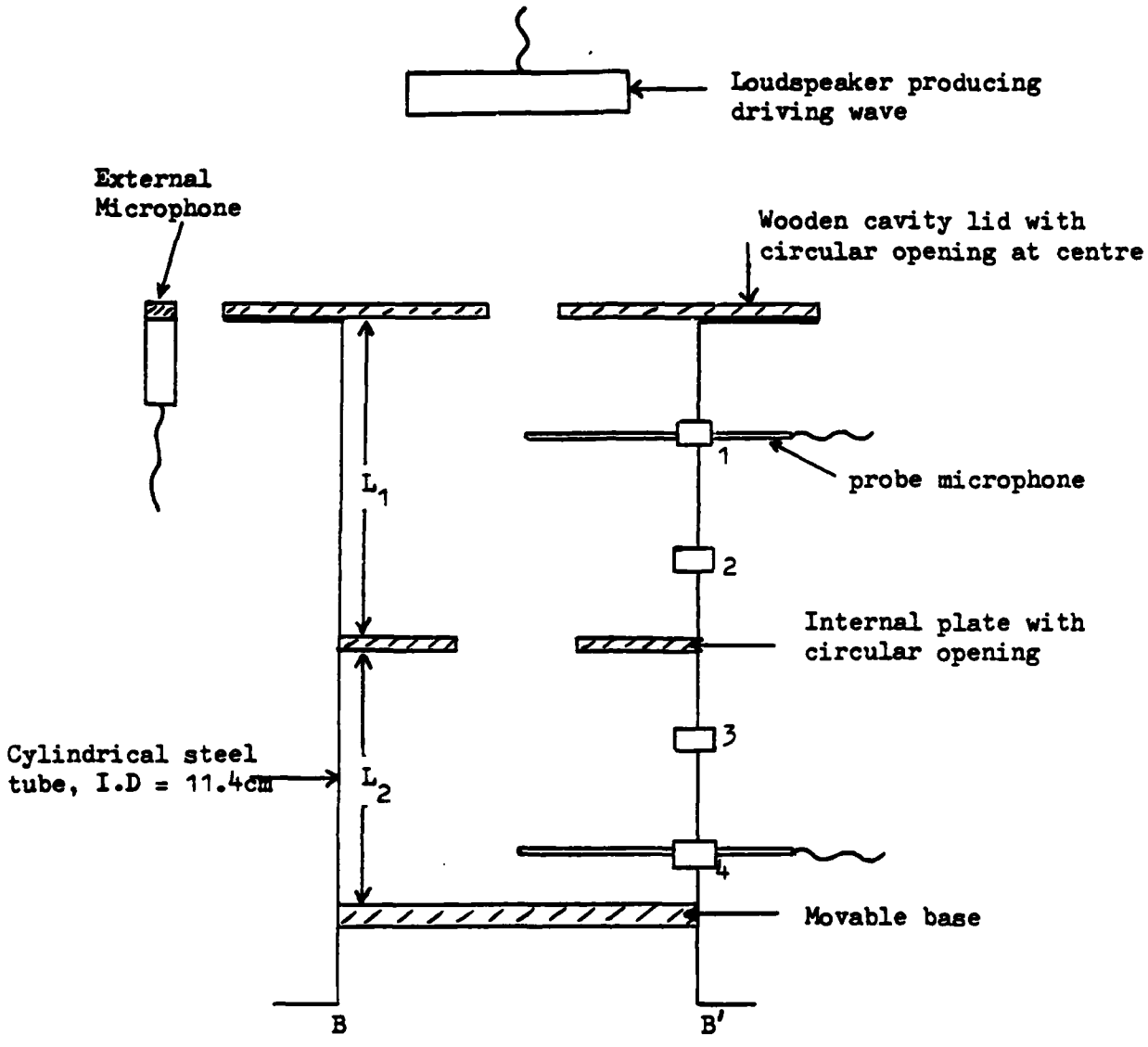

FIGURE 1 ILLUSTRATION OF CYLINDRICAL CAVITY SYSTEM TESTED IN ANECHOIC CHAMBER

The cavity consists of a cylindrical steel tube of 11.4 cm internal diameter having a flanged opening at one end over which can be fitted any one of a number of wooden lids, 0.6 cm thick, containing circular openings of various diameters. The cylinder has a moveable base whose height can be adjusted to vary the length of the cavity. The maximum length attainable is 63.6 cm. Any one of a number of circular wooden plates, containing circular concentric holes of various diameters, can be inserted into the cylinder as shown above to create a two-cavity system. The diameters of the holes in both the lids and the internal plates range from 0.2 cm to 8 cm.

The external excitation of the system was provided by an electrostatic loudspeaker suspended above the cavity, driven by an oscillator producing a sinusoidal tone of variable frequency. Sound pressure levels (SPLs)

inside the cavity were measured by probe microphones as shown in Figure 1. These could be placed at any of four axial positions via openings in the tube wall, numbered 1 to 4 in the diagram. Each opening was blanked off when not in use. The heights of the openings relative to the lower end of the cylinder (BB' in Figure 1) are given in Table 1 below.

Probe position (Fig 1)	Height above lower end (cm)
1	56.2
2	37.6
3	19.0
4	6.6

TABLE 1 Probe Microphone Positions

Two probe microphones were used in the experiments, enabling the response to be measured at two positions simultaneously. Not all four positions were used for each configuration studied, although this was done in a few cases. The SPL external to the cavity was measured by a $\frac{1}{2}$ inch microphone placed in the plane of the lid, 18 cm from the central axis. No measurements were made at frequencies above 1kHz because interest was centred on the first few resonant frequencies of the system, these being the ones which would be most easily excited by an external flow. In most cases the measurements were confined to the range 50 to 700Hz. No measurements were made below 50Hz because of the low efficiency of the loudspeaker at low frequencies and the absence of anechoic conditions in the chamber for long acoustic wavelengths.

Three cavity configurations were examined. These were:

i) No internal plate (ie single cavity), cavity length = 63.6 cm.

ii) No internal plate, cavity length = 32.0 cm.

iii) Internal plate giving L_1 = upper cavity length = 31.9 cm, and L_2 = lower cavity length = 31.1 cm.

Several opening diameters were investigated with each of the above three configurations. The measurement procedure was as follows. A discrete frequency was chosen and set up on the oscillator, the level being adjusted until the external microphone gave an output corresponding to a reference acoustic pressure of 120dB re 1 μPa. The corresponding SPLs at the internal microphones were then recorded. This procedure was repeated for a range of discrete frequencies, thus building up a frequency response in the range of interest. Small steps in frequency were taken near resonances of the system, where the SPL measured by the probe microphones was changing rapidly with frequency.

Before proceeding to a discussion of the experimental results a description is given of the theoretical modelling of the system. Experimental and theoretical results are then presented together in section 2 (c).

(b) Theoretical Model

i) Formulation.

In constructing a mathematical model of the system a more general geometry has been considered, with allowance for upper and lower cavities having different diameters as shown in Figure 2.

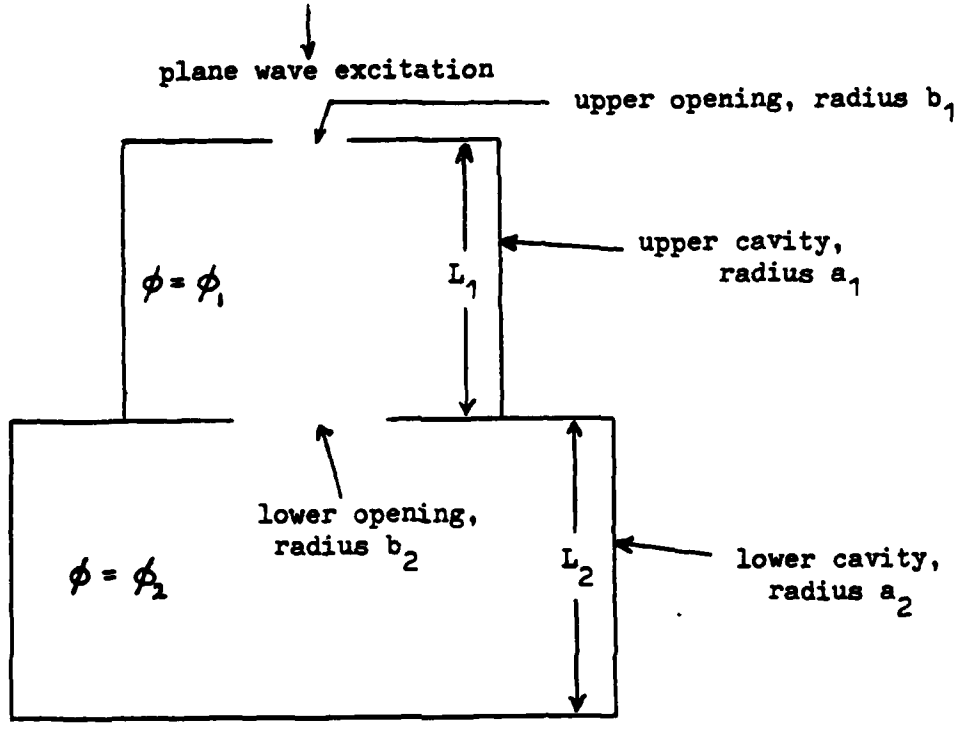

FIGURE 2 GEOMETRY OF THEORETICAL MODEL

A cylindrical polar coordinate system is used, with the origin at the centre of the lower opening. Thus the upper opening is at $z = L_1$, the lower opening at $z = 0$ and the base of the lower cavity at $z = -L_2$. The notation is as follows:

a	=	radius of cylinder
b	=	radius of opening
c	=	sound speed
f	=	frequency (Hz)
k	=	wave number $= \omega/c$
K	=	damping parameter
L	=	cavity length
M	=	mass of fluid in opening
p	=	acoustic pressure
r	=	radial coordinate
t	=	time
z	=	axial coordinate
ν	=	kinematic viscosity
ρ	=	density
τ	=	thickness of opening
ϕ	=	velocity potential
ω	=	radian frequency

Subscripts 1 and 2 refer to the upper and lower cavities respectively. Subscript 0 refers to the external excitation, assumed to be a plane wave of velocity amplitude u_0. Thus the driving wave is described by the velocity potential

$$\phi_0 = \frac{u_0}{k} e^{ik(ct+z-L_1)} . \tag{2.1}$$

Inside each cavity it is required to find a solution of the Helmholtz equation,

$$(\nabla^2 + k^2)\phi = 0, \tag{2.2}$$

subject to the appropriate boundary conditions. Since the walls are all rigid we may write

$$\frac{\partial \phi}{\partial r} = 0 \text{ on } r = a_1 \ (z>0) \text{ and on } r = a_2 \ (z<0);$$

$$\frac{\partial \phi}{\partial z} = 0 \text{ at } z = L_1 \ (\text{for } b_1 < r \leq a_1),$$

$$\text{at } z = 0^+ \ (\text{for } b_2 < r \leq a_1), \text{ at } z = 0^- \ (\text{for } b_2 < r \leq a_2) \tag{2.3}$$

$$\text{and at } z = -L_2 \ (\text{for } r \leq a_2).$$

It remains to write appropriate boundary conditions for the motions in the openings at $z = L_1$ and $z = 0$. In each opening the motion is assumed to be that of a rigid piston oscillating with frequency ω. Consider first the upper opening. Some of the input energy is lost from this opening to the external fluid via radiation. The external fluid also has a reactive effect due to its mass. These effects may be combined in the form of a specific acoustic impedance, $\theta_1 + i\chi_1$. That is, if a motion in the mouth with acoustic velocity u_1 induces a mean acoustic pressure p' just outside the opening, we write

$$\frac{p'}{u_1} = \rho c (\theta_1 + i\chi_1). \tag{2.4}$$

Expressions for the resistance and reactance terms, θ_1 and χ_1, are obtained on the assumption that the motion in the opening is that of a piston in an open-ended tube with no baffle. (It can be seen from Figure 1 that the lid of the cavity is in fact a baffle, but its size is less than the wavelengths of interest, so its effect has been ignored). For low frequencies ($kb_1 << 1$), χ_1 and θ_1 are given [3] by

$$\chi_1 = \frac{2}{\pi}(kb_1), \quad \theta_1 = \frac{1}{4}(kb_1)^2. \tag{2.5}$$

Now the velocity u_1 is simply the mean value of $\partial\phi_1/\partial z$ at $z = L_1$, averaged over the mouth area. Denoting this average by an overbar, the total mean acoustic pressure just outside the upper opening is given by

$$\overline{p}_{out} = \text{driving pressure} + p'$$

$$= -\rho i c u_0 + \rho c (\theta_1 + i\chi_1) \overline{\frac{\partial \phi_1}{\partial z}}, \qquad (2.6)$$

where it is understood that all quantities vary as $e^{i\omega t}$. The mean pressure just inside the opening is given by

$$\overline{p}_1 = -\rho \overline{\frac{\partial \phi_1}{\partial t}} = -\rho i\omega \overline{\phi}_1 . \qquad (2.7)$$

The equation of motion of the fluid mass M_1 in the upper opening is now written as

Mass X acceleration = nett pressure force - viscous damping force.

It can be shown [4] that the viscous damping term is proportional to $\rho u_1 \sqrt{\nu\omega}$, where ν is the kinematic viscosity. Hence we may write

$$M_1 \frac{du_1}{dt} = A_1 (\overline{p}_1 - \overline{p}_{out}) - K A_1 \rho u_1 \sqrt{\nu\omega}, \qquad (2.8)$$

where A_1 is the mouth area and K is a parameter dependent on the geometry of the opening, whose value is discussed later. Since

$$\frac{du_1}{dt} = i\omega u_1 = i\omega \overline{\frac{\partial \phi_1}{\partial z}},$$

the above equation may be written in the form

$$\left[(\chi_1 + k\tau_1) - i\left(\theta_1 + K\sqrt{\frac{ka_1}{R}}\right)\right] \overline{\frac{\partial \phi_1}{\partial z}} + k\overline{\phi}_1 = u_0, \qquad (2.9)$$

where τ_1 is the effective opening thickness $= M_1/(\rho A_1)$, and $R = a_1 c/\nu$. The dimensionless parameter R is analogous to a Reynolds number, but it involves the sound speed rather than a characteristic flow speed. Equation (2.9) represents the boundary condition to be applied at the upper opening. That is, at $z = L_1$, $0 \leq r \leq b_1$.

In the same way an equation can be written for the motion of the mass in the lower opening. With similar notation, this takes the form

$$M_2 \frac{du_2}{dt} = A_2 (\overline{p}_2 - \overline{p}_1) - K A_2 \rho u_2 \sqrt{\nu\omega}. \qquad (2.10)$$

In this equation $\overline{p}_2$ and $\overline{p}_1$ refer to the mean acoustic pressures below and above the opening at z = 0. When expressed in terms of the velocity potentials, (2.10) takes the form

$$\left[k\tau_2 - iK\sqrt{\frac{ka_1}{R}}\right] \overline{\frac{\partial \phi_1}{\partial z}} + k(\overline{\phi}_2 - \overline{\phi}_1) = 0. \qquad (2.11)$$

This is the boundary condition at $z = 0$ for $0 \leq r \leq b_2$, together with the condition $\overline{\partial\phi_1/\partial z} = \overline{\partial\phi_2/\partial z} = u_2$. The velocities u_1 and u_2 are to be determined as part of the solution.

It should be noted that the thicknesses of the lid and the internal plate have been ignored in this formulation except in the allowance for non-zero effective mouth thicknesses at $z = 0$ and $z = L_1$. Also, viscous losses are assumed to occur only at the openings. That is, energy dissipation within the cavities has been neglected.

ii) Solution.

The solution of the Helmholtz equation is now written, for each cavity, as a sum of eigenfunctions. In the upper cavity we write

$$\phi = \phi_1 = \sum_{n=1}^{\infty} \left[A_n g_{1n}(z) + B_n h_{1n}(z)\right] J_0\left(\frac{r}{a_1}\xi_n\right), \qquad (2.12)$$

where the ξ_n are the roots of $J_0'(\xi_n) = 0$ and the functions g_{1n}, h_{1n} are sinusoidal or exponential depending on whether $ka_1 > \xi_n$ or $ka_1 < \xi_n$. That is,

$$g_{1n}(z) = \begin{cases} \cos(\mu_n z/a_1), & ka_1 \geq \xi_n \\ \exp(-\mu_n z/a_1), & ka_1 < \xi_n \end{cases},$$

$$h_{1n}(z) = \begin{cases} \sin(\mu_n z/a_1), & ka_1 \geq \xi_n \\ \exp(\mu_n z/a_1), & ka_1 < \xi_n \end{cases}, \qquad (2.13)$$

where $\mu_n = \left|\xi_n^2 - (ka_1)^2\right|^{1/2}$.

The change from exponential to sinusoidal behaviour as ka_1 increases reflects the well-known fact that the propagation of duct modes is frequency dependent. Since $\xi_1 = 0$ the plane wave, independent of r, always propagates (independently of frequency) in a hard walled tube, but the second and higher modes do not become "cut on" unless the frequency is sufficiently high. The second mode begins to propagate for $ka_1 > 3.83$, which is the first non-zero root of $J_0'(\xi) = 0$. In the present case, with $a_1 = 5.7$ cm, this corresponds to a frequency of about 3.6 kHz which is well above the range of interest. The solution given by (2.12) is valid in $0 \leq z \leq L_1$, $0 \leq r \leq a_1$. The determination of the coefficients A_n and B_n, which are chosen to satisfy the boundary conditions at $z = 0$ and $z = L_1$, is given later in this section.

The form of solution given by equation (2.12) is axisymmetric, ignoring any variation with the circumferential angle θ. A more general solution could be written involving terms of the form $e^{im\theta}$ and the higher order Bessel functions J_m. However, the experimental rig described previously is axisymmetric, so the general solution is not used here.

The solution for ϕ_2, valid in the lower cavity, has a similar form to that given above for ϕ_1. Since $\partial\phi_2/\partial z = 0$ at $z = -L_2$, ϕ_2 may be written as

$$\phi_2 = \sum_{n=1}^{\infty} C_n g_{2n}(z) J_0\left(\frac{r}{a_2}\xi_n\right) , \qquad (2.14)$$

where $$g_{2n}(z) = \begin{cases} \cos[\eta_n(z+L_2)/a_2], & ka_2 \geq \xi_n \\ \cosh[\eta_n(z+L_2)/a_2], & ka_2 < \xi_n \end{cases} \qquad (2.15)$$

and $$\eta_n = \left|\xi_n^2 - (ka_2)^2\right|^{1/2} .$$

It remains to choose A_n, B_n and C_n to satisfy the remaining boundary conditions. It has been assumed that the fluid particles in each opening vibrate as a rigid piston, so the acoustic velocities at $z = 0$ and $z = L_1$ are written as

$$\left.\frac{\partial \phi_1}{\partial z}\right|_{z=L_1} = \begin{cases} u_1 , & r \leq b_1 \\ 0 , & r > b_1 \end{cases} ,$$

$$\left.\frac{\partial \phi_1}{\partial z}\right|_{z=0} = \left.\frac{\partial \phi_2}{\partial z}\right|_{z=0} = \begin{cases} u_2, & r \leq b_2 \\ 0 , & r > b_2 \end{cases} . \qquad (2.16)$$

A result from the theory of Hankel transforms [5] states that, if $f(r)$ is a function defined in $0 \leq r \leq a$, with $f'(a) = 0$, then $f(r)$ can be written as

$$f(r) = \sum_{1}^{\infty} F_n J_0\left(\frac{r}{a}\xi_n\right) ,$$

where $$F_n = \frac{2}{a^2 J_0^2(\xi_n)} \int_0^a r f(r) J_0\left(\frac{r}{a}\xi_n\right) dr .$$

Defining $f(r) = \left.\frac{\partial \phi_1}{\partial z}\right|_{z=L_1}$, it is seen that

$$A_n g_{1n}'(L_1) + B_n h_{1n}'(L_1) = \frac{2}{a_1^2 J_0^2(\xi_n)} \int_0^{b_1} r u_1 J_0\left(\frac{r}{a_1}\xi_n\right) dr$$

$$= \frac{2\left(\frac{b_1}{a_1}\right) u_1 J_1\left(\frac{b_1}{a_1}\xi_n\right)}{\xi_n J_0^2(\xi_n)} . \qquad (2.17)$$

Similarly, consideration of conditions at z = 0 gives two further equations, namely

$$A_n g_{1n}'(0) + B_n h_{1n}'(0) = \frac{2\left(\frac{b_2}{a_1}\right) u_2 J_1\left(\frac{b_2}{a_1}\xi_n\right)}{\xi_n J_0^2(\xi_n)} \qquad (2.18)$$

and

$$C_n g_{2n}'(0) = \frac{2\left(\frac{b_2}{a_2}\right) u_2 J_1\left(\frac{b_2}{a_2}\xi_n\right)}{\xi_n J_0^2(\xi_n)} . \qquad (2.19)$$

Consider now the boundary conditions (2.9) and (2.11), which are averaged over the mouth areas. Defining

$$\alpha = \chi_1 + k\tau_1 , \quad \beta = \theta_1 + K\sqrt{\frac{ka_1}{R}} ,$$

equation (2.9) becomes

$$(\alpha - i\beta) u_1 + \frac{k}{\pi b_1^2} \int_0^{b_1} 2\pi r \phi_1 \, dr = u_0 . \qquad (2.20)$$

Similarly, with $\gamma = k\tau_2$ and $\delta = K\sqrt{ka_1/R}$, (2.11) becomes

$$(\gamma - i\delta) u_2 + \frac{k}{\pi b_2^2} \int_0^{b_2} 2\pi r (\phi_2 - \phi_1) \, dr = 0 . \qquad (2.21)$$

Using the expressions given earlier for ϕ_1 and ϕ_2, equations (2.17) to (2.21) may be solved to give A_n, B_n, C_n, u_1 and u_2, thus completing the solution. The appropriate expressions are given in the Appendix.

With all coefficients determined the velocity potential, and hence the acoustic pressure, may be found at any point in either cavity as a function of frequency. The coefficients are of course frequency dependent, so a separate computation must be performed for each frequency of interest. Dimensionless velocity potential and acoustic pressure are defined by

$$\hat{\phi} = \frac{\phi}{a_1 u_0} , \quad \hat{p} = \frac{p}{\rho c u_0} . \qquad (2.22)$$

The SPL at any point inside a cavity, in relation to the driving pressure p_0, is then given by

$$SPL = 20 \log_{10}[(ka_1)|\hat{\phi}(r,z)|] . \qquad (2.23)$$

It remains to correct this expression to allow for the fact that the pressure measured by the external microphone, shown in Figure 1, is not equal to the plane wave driving pressure p_o, but also contains a component due to radiation from the upper opening. This component is calculated on the assumption that the opening radiates as though it were the open end of an unbaffled tube. That is, the motion in the mouth with velocity u_1 is regarded [3] as the sum of a dipole and a piston in an infinite baffle, each having velocity $\frac{1}{2} u_1$, as sketched in Figure 3 below.

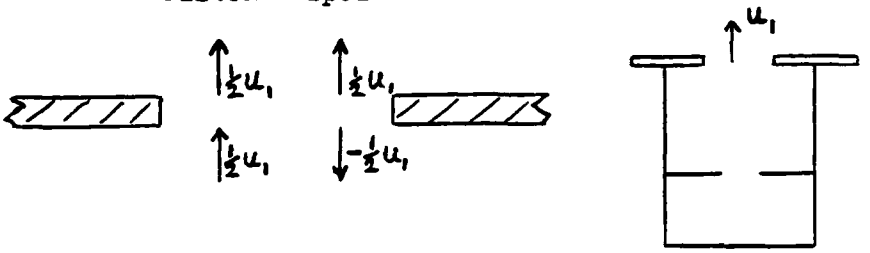

FIGURE 3 MODELLING OF MOTION IN UPPER MOUTH

Above the opening the piston and dipole components add to give a motion of amplitude u_1, while beneath the opening the components cancel, thus ensuring no radiation from below the mouth. The dipole component produces no radiation in the plane of the lid, so the signal received at the external microphone is that which would be produced by a piston in an infinite baffle, having velocity $\frac{1}{2} u_1 e^{i\omega t}$. The radiation pattern due to such a motion is well known [4], and for $kb_1 << 1$ the pressure at distance R from the centre of the opening is given approximately by

$$p(R) \simeq \frac{i\rho\omega b_1^2 u_1}{4R} e^{i(\omega t - kR)} . \qquad (2.24)$$

Hence, ignoring the $e^{i\omega t}$ term, the total acoustic pressure p_E at the external microphone is given by

$$p_E(R) = p_o + \frac{i\rho\omega b_1^2 u_1}{4R} e^{-ikR} ,$$

which in dimensionless terms becomes

$$\hat{p}_E = -i\left[1 - \frac{(ka_1)\left(\frac{b_1}{a_1}\right)^2 \left(\frac{u_1}{u_o}\right) e^{-ikR}}{4\,(R/a_1)}\right] . \qquad (2.25)$$

The relative pressure between an internal point and the external microphone position is then given by

$$SPL = 20\log_{10}[ka_1|\hat{\phi}|] - 20\log_{10}|\hat{p}_E| . \qquad (2.26)$$

A number of approximations have been made which give rise to uncertainty in the prediction of SPL from the above equation. Firstly, the motion has been assumed uniform over the mouth area, and secondly the effect of the finite size of the lid has been ignored. These approximations cause inaccuracies, both in the expression for p_E and in the values of χ_1 and θ_1, given in equation (2.5). The reactance χ_1 is given by (2.5) as $2(kb_1)/\pi$, which is appropriate to an open-ended tube with no baffle. Its true value is expected to lie somewhere between this value and $8(kb_1)/3\pi$, which is the value appropriate to an infinite baffle. These two extreme values differ by 33%, and although a variation of this order can have a significant effect on predicted absolute sound pressure levels (typically of up to about 3dB at resonance), the predictions of relative acoustic pressure between coupled cavities are unaltered. The same is true of variations in the value of the radiation resistance θ_1. This point is discussed further in Section 2(d). Similarly, an error in the correction term in (2.25) cannot affect relative SPLs. Since $R/a_1 = 3.15$ ($R = 18$ cm), and $ka_1 \leq 1$ for frequencies below 1kHz, the correction term is negligible for most frequencies, although it can become significant in the immediate vicinity of resonance, when $|u_1/u_0|$ is large. Thus the main errors are expected to occur in the prediction of absolute SPL at resonance rather than in relative SPLs within the cavities.

The energy losses due to radiation and viscosity can be written in terms of the acoustic velocities u_1 and u_2 at the upper and lower openings. Consideration of the energy balance in the system leads to the expression

$$\tfrac{1}{2}\rho c A_1 u_0 \mathrm{Im}(u_1) = \tfrac{1}{2}\rho A_1 \left[c\theta_1 + K\sqrt{\nu\omega}\right]|u_1|^2 + \tfrac{1}{2}K\rho A_2\sqrt{\nu\omega}\,|u_2|^2 . \qquad (2.27)$$

The left-hand side of the above is the nett rate of input of energy to the system by the driving wave, and the two terms on the right represent the rates of energy loss at the upper and lower openings. The loss at the upper opening is the sum of a viscous loss and a radiation loss, while the loss at the lower opening is purely viscous. In order to calculate the system response some estimate must be made of the value of K. A study of the mouth impedance of a Helmholtz resonator has been carried out by Hersh and Walker [6], who give the following expression for a cylindrical cavity exposed to a small amplitude driving pressure:

$$K = \frac{6{\cdot}4(\tau_e/d)^2}{1 + 3(\tau/d)} , \qquad (2.28)$$

where d = mouth diameter (= 2b in the present notation)
and τ_e = effective mouth thickness, given by

$$\tau_e = \tau + \frac{0{\cdot}85\,d}{1 + 0{\cdot}625(d/D)} .$$

Here D is the cavity diameter. The above expression was derived by Hersh and Walker from experimental data measured in the range $0.035 \leq \tau/d \leq 0.287$, $0.093 \leq d/D \leq 0.187$. Some of the present experiments were carried out with τ/d and d/D outside these ranges, so exact agreement with equation (2.28) cannot be expected. A further discrepancy arises from the fact that some of the present measurements correspond to excitation amplitudes outside the strictly linear regime as defined by Hersh and Walker, who state that the effect of nonlinearity is to increase the effective value of K. Hence the present results are expected to correspond to a damping parameter K greater than or equal to the value given by (2.28). A detailed discussion of the experimental results, including their dependence on the damping parameter, is given in the following section.

c) Comparison of Theory and Experiment.

i) Single Cavity. Before discussing the behaviour of coupled cavities it is instructive to consider some of the results obtained for the relatively simple case of a single cavity. Two single-cavity lengths were examined, with L_1 = 63.6 cm and 32.0 cm. A number of mouth radii were tried in each case. Typical experimental results are presented below and are compared with theoretical predictions. Tables 2 and 3 show measured and predicted resonant frequencies in the single-cavity cases, for a number of mouth radii.

b_1 (cm)	b_1/a_1	f_1 (Hz)		f_2 (Hz)		f_3 (Hz)		f_4 (Hz)	
		Expt	Theory	Expt	Theory	Expt	Theory	Expt	Theory
2.5	0.437	107	108	335	336	582	583	841	840
0.75	0.131	62	64	286	287	547	547	813	814
0.25	0.044	-	31	272	273	539	540	808	810

TABLE 2 Experimental and Theoretical Values of First Four Resonant Frequencies for Single Cavity with L_1 = 63.6 cm.

b_1 (cm)	b_1/a_1	f_1 (Hz)		f_2 (Hz)	
		Expt	Theory	Expt	Theory
1.5	0.262	139	142	574	580
0.5	0.087	69	74	541	545
0.25	0.044	-	43	533	539

TABLE 3 Experimental and Theoretical Values of First Two Resonant Frequencies for Single Cavity with L_1 = 32.0 cm.

The lowest resonant frequency (f_1) was not measured with b_1 = 0.25 cm, since measurements were made only above 50Hz. Agreement between theory and experiment is seen to be very good. There is a tendency to slightly over-predict the resonant frequencies, but the errors are small, particularly for the longer of the two cavities. Measurements of internal SPL were made at all four microphone positions for the case L_1 = 63.6 cm, b_1 = 0.75 cm. For this case the relative sound pressure level between microphone positions 1 and 4 (as defined in Table 1) is plotted against frequency in Figure 7. Four frequency ranges were covered, chosen to include the first four resonant frequencies. Good agreement is again obtained between measured and predicted values, but the experimental values tend to vary rather erratically in the immediate neighbourhoods of the second, third and fourth resonances. This points to a degree of inaccuracy in the measurements very close to resonance, which can be attributed to the fact that the resonances were very sharply tuned, each of the measured SPL values varying rapidly with frequency near resonance. In Figure 7, and throughout this section, the notation p_1, .., p_4 is used to denote the SPLs measured at the four internal microphone positions.

Typical predictions of the variation of cavity pressure with frequency are plotted in Figures 8 and 9, where p_1/p_E and p_2/p_E are given as functions of frequency, in the range 50 to 700Hz, for the shorter cavity (L_1 = 32 cm) with b_1 = 1.5 cm and 0.5 cm. Here p_E is the reference pressure at the external microphone. In these cases internal measurements could be made only at positions 1 and 2, since the movable base is above the level of position 3 when L_1 = 32 cm. Agreement with the measured values is seen to be fairly good over most of the frequency range examined. In predicting the system response for these cases the value of the damping parameter K was found from equation (2.28). The effective values of K are evidently greater than (2.28) predicts since the theoretical maximum system response at resonance is consistently over-predicted. The discrepancy is particularly marked at the second resonance in Figure 9, indicating a much higher effective value of K than the figure of 4.52 found from (2.28). There are a number of reasons for the lack of agreement. It has already been remarked that the approximate treatment of the motion in the mouth gives rise to uncertainty in the predictions, which can be important near resonance. In addition equation (2.28) is strictly meant to apply only to a Helmholtz resonator, so it may not be valid for higher modes of resonance.

ii) Coupled Cavities. The above discussion of single cavities has shown the difficulty in estimating the effective damping, so that the theory presented here is not able to predict consistently accurate values of absolute SPL close to resonant frequencies. However, the main purpose of the present study is to examine the relative SPL between coupled cavities, and it is now shown that sound transmission between resonating cavities is almost independent of the damping for most cases of practical interest. Consider, for example, the case of two coupled cavities with L_1 = 31.9 cm, L_2 = 31.1 cm, b_1 = 1 cm and b_2 = 0.5 cm. The frequency response was calculated for this case

using two widely differing values of K, K = 30 and K = 3.83. (Equation (2.28) gives K = 3.83 for b = 1 cm and 4.52 for b = 0.5 cm. The lower value was chosen for comparison with K = 30). Measurements were made at positions 2 and 4 (ie one probe in each cavity), in the range 50 to 630Hz. The computed pressure ratio p_4/p_2 is plotted in Figure 10 for these values of K, together with the measured values. The maxima of p_4/p_2 shown in Figure 10 should not be confused with the resonant frequencies (which are marked on the graph as f_1, .., f_4). The peaks are due to antiresonances, defined by the occurrence of minima in p_2. In the high frequency range (500 to 630Hz) the difference between the predictions for the two values of K is too small to be plotted, so only one line is shown on the graph. In the low frequency range (50 to 200Hz) the difference between the predictions is seen to be small except in the vicinity of the antiresonance. (No results are presented in the range 200 to 500Hz because of the absence of resonances in that range). The explanation for the dependence of p_4/p_2 on K is given later in this section, where a simplified model of coupled cavities is presented. The main point to note here is that, over most of the frequency range, including the resonant frequencies, the relative SPL between the cavities is virtually independent of the damping, at least in the range $3.83 \leqslant K \leqslant 30$. The true effective value of K for this case lies somewhere between these two extremes. This is seen from the measured maximum of p_4/p_2 in the low frequency range (13.5dB at 82Hz), which lies between the two theoretical values for the low and high values of K.

In the case of a very small opening (b_1 = 1mm), measurements were attempted for the case of a single cavity with L_1 = 63.6 cm, but the internal pressure levels were very low and could not be measured accurately, so no estimate of the effective value of K could be made. Furthermore the values of t/d (=3) and d/D (= 0.0175) lie well outside the ranges for which equation (2.38) is judged to be valid. Thus no reliable data are available from which to predict the effect of viscosity on relative SPL when the size of opening is very small. It may be that viscosity has a significant effect in such cases, but this size of opening is not of great practical interest, so the investigation of very small openings was not pursued further.

It should be noted that, although the damping is unimportant in determining the relative SPL between resonating cavities when the size of the connecting opening is of the order of 1 cm or more, the absolute levels in the cavities depend critically on the damping. When the system is excited at any fixed frequency, a steady state is reached when the rate of energy dissipation balances the nett input from the driving wave. If K is very small a high value of acoustic velocity must be attained in the mouth before the dissipation rate balances the input. This produces a correspondingly large SPL inside each cavity, even though the ratio of the acoustic pressures in the cavities is virtually independent of viscosity.

Returning now to Figure 10, it is seen that the agreement between theory and experiment is generally poor, and cannot be

improved by an appropriate choice of K. However, if the effective mass of fluid in the lower opening is allowed to vary from the static value of $\rho(\pi b_2^2)\tau_2$, calculated on the basis of the geometric opening thickness, then considerably improved agreement can be obtained. This can be seen from Figure 11, where p_4/p_2 is plotted against frequency for different values of effective mouth thickness τ_2, with K = 10. In the low frequency range predictions are shown for τ_2 = 6 mm (the geometric value), for τ_2 = 0, and for the intermediate value of τ_2 = 2.4 mm. Good agreement is obtained with the measurements when the latter value is used. In the high frequency range, covering the third and fourth resonances, good overall agreement is obtained with τ_2 = 0. By letting the effective opening thickness vary as shown in Figure 11, improved agreement is also obtained between measured and predicted resonant frequencies. This is illustrated in Table 4 below.

	f_1	f_2	f_3	f_4
Measured Value (Hz)	57	148	559	591
Theory, τ_2 = 0	63	161	557	590
Theory τ_2 = 2.4 mm	60	152	557	583
Theory τ_2 = 6 mm	56	146	556	577

TABLE 4 Measured and Predicted Resonant Frequencies of Coupled Cavities with b_1 = 1 cm, b_2 = 0.5 cm, L_1 = 31.9 cm, L_2 = 31.1 cm.

The most marked effect of setting τ_2 to zero is to reduce the error in the predicted value of f_4 from 14Hz to 1Hz. The frequency of the third mode is virtually independent of τ_2, and the errors in prediction of f_1 and f_2 are not greatly altered when τ_2 is reduced from 6 mm to 2.4 mm.

The above results, together with those presented in Figure 11, show that the effective mouth thickness (ie the effective mass of fluid in the opening) is to some extent frequency dependent, and is not simply equal to the geometric value. This is not altogether surprising in view of the approximate treatment of the motion in the mouth, which is regarded as that of a rigid piston.

The measured responses of the individual microphones at positions 2 and 4 are plotted in Figure 12, together with theoretical predictions for which K was arbitrarily set equal to 10. The overall agreement is considered reasonable in view of the approximations discussed earlier.

The same trends are observed with all the coupled cavity cases, so no other case is presented in detail. Agreement between theory and experiment improves when the effective mass of fluid in the opening connecting the cavities is reduced from

its static value, and in each case the relative SPL between the cavities is virtually independent of viscosity except near an anti-resonance.

(d) Simplified Theoretical Model.

The theory presented in Section 2(b) is valid over a wide range of frequencies, but suffers from the deficiency of being too complex for easy interpretation of some of the results. It was therefore felt worthwhile to develop a simpler model capable of easier interpetation, even though its range of validity would be confined to low frequencies. The model is simply an extension to coupled cavities of the classical Helmholtz resonator. The system is therefore represented as a series of masses and springs, as illustrated in Figure 4 below.

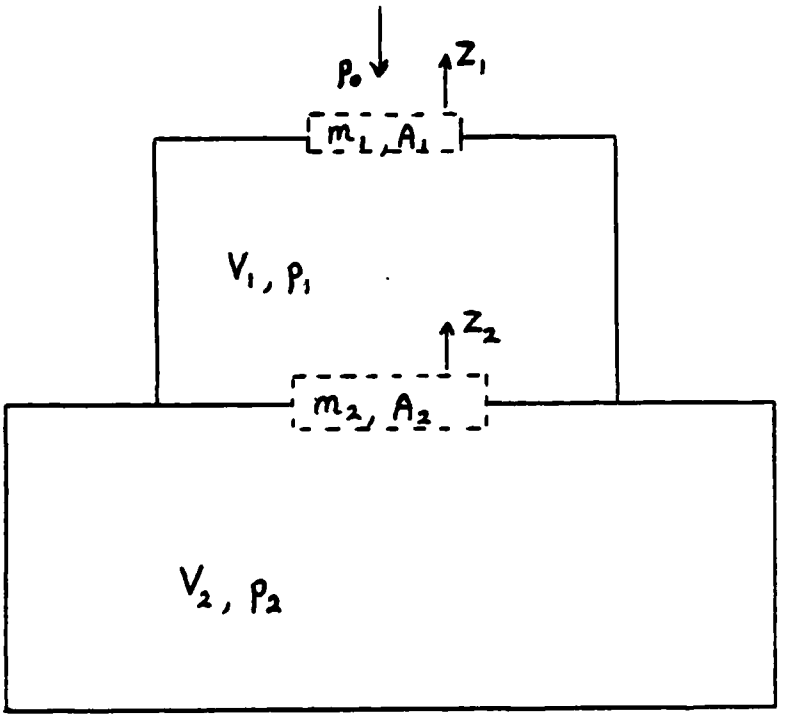

FIGURE 4 SIMPLE MODEL OF TWO COUPLED CAVITIES WITH RIGID WALLS

The notation is as follows:

A	=	mouth area
m	=	effective mass of fluid in mouth
p	=	acoustic pressure
Z	=	displacement of fluid in mouth (positive upwards)
γ	=	damping coefficient
V	=	cavity volume

The subscripts 1 and 2 refer to the upper and lower cavities as in Section 2(b), and are no longer related to the probe microphone positions.

The pressure is assumed to be uniform throughout each cavity, so the model is valid only for acoustic wavelengths which are large in relation to the cavity dimensions.

Let the mass m_1 in the upper opening be subject to an oscillating driving pressure p_o. Then the equation of motion of m_1 is written as

$$m_1 \frac{d^2 Z_1}{dt^2} = A_1(p_1 - p_o) - \gamma_1 \frac{dZ_1}{dt} , \tag{2.29}$$

where the damping force is assumed to be linear in the velocity, as in the previous model. Similarly, the equation for m_2 is

$$m_2 \frac{d^2 Z_2}{dt^2} = A_2(p_2 - p_1) - \gamma_2 \frac{dZ_2}{dt} . \tag{2.30}$$

The displacement of the fluid masses in the cavity openings gives rise to corresponding volume changes ΔV_1 , ΔV_2 of the fluid in each cavity. The pressure changes in each cavity are related to these volume changes by

$$p_1 = -\frac{\rho c^2}{V_1}\Delta V_1 = -\frac{\rho c^2}{V_1}[A_1 Z_1 - A_2 Z_2] , \tag{2.31}$$

$$p_2 = -\frac{\rho c^2}{V_2}\Delta V_2 = -\frac{\rho c^2}{V_2}(A_2 Z_2) . \tag{2.32}$$

If the pressures and displacements are now assumed all to vary as $e^{i\omega t}$, then substitution of (2.31) and (2.32) into the equations of motion of the masses gives

$$-m_1\omega^2 Z_1 + i\gamma_1\omega Z_1 + \frac{A_1\rho c^2}{V_1}[A_1 Z_1 - A_2 Z_2] = -A_1 p_o , \tag{2.33}$$

$$-m_2\omega^2 Z_2 + i\gamma_2\omega Z_2 + A_2^2\rho c^2\left(\frac{1}{V_1}+\frac{1}{V_2}\right)Z_2 - \frac{A_1 A_2 \rho c^2}{V_1} Z_1 = 0 . \tag{2.34}$$

Setting

$$\alpha = \frac{A_1^2\rho c^2}{V_1} - m_1\omega^2 + i\omega\gamma_1 ,$$

$$\beta = A_2^2\rho c^2\left(\frac{1}{V_1}+\frac{1}{V_2}\right) - m_2\omega^2 + i\omega\gamma_2 ,$$

the solution for Z_1 and Z_2 is given by

$$Z_1 = -\frac{A_1 p_o}{\Gamma}\beta , \quad Z_2 = -\frac{A_1 p_o}{\Gamma}\left(\frac{A_1 A_2 \rho c^2}{V_1}\right) , \tag{2.35}$$

where $$\Gamma = \alpha\beta - \left(\frac{A_1 A_2 \rho c^2}{V_1}\right)^2 .$$

The acoustic pressures p_1 and p_2 are then found from

$$\frac{p_1}{p_0} = \frac{A_1^2 \rho c^2}{\Gamma V_1}\left(\frac{A_2^2 \rho c^2}{V_2} - m_2\omega^2 + i\omega\gamma_2\right),$$

$$\frac{p_2}{p_0} = \frac{(A_1 A_2 \rho c^2)^2}{\Gamma V_1 V_2} . \qquad (2.36)$$

The pressure ratio between the cavities is therefore given by

$$\frac{p_1}{p_2} = 1 + \frac{V_2}{A_2^2 \rho c^2}(-m_2\omega^2 + i\omega\gamma_2) . \qquad (2.37)$$

A number of features of the solution can immediately be deduced from the above expressions. Firstly, the pressure ratio p_1/p_2 is independent of all quantities associated with the upper cavity. Hence variations in the effective mass or damping at the upper opening do not affect the relative SPL between the cavities. Also there are two resonant frequencies, defined by minima of $|\Gamma|$. For lightly damped systems these frequencies may be found by setting $\gamma_1 = \gamma_2 = 0$ and solving the equation $\Gamma = 0$, which is a quadratic in ω^2.

It can be seen from (2.37) that $|p_1/p_2|$ has a minimum at the frequency given by

$$\omega^2 = \frac{A_2^2 \rho c^2}{m_2 V_2} . \qquad (2.38)$$

At this frequency we have

$$\left|\frac{p_1}{p_2}\right|_{min} = \frac{\omega\gamma_2 V_2}{A_2^2 \rho c^2} , \text{ and } \quad \frac{A_1 Z_1}{A_2 Z_2} = 1 + \frac{i\omega\gamma_2 V_1}{A_2^2 \rho c^2} . \qquad (2.39)$$

That is, the displacements Z_1 and Z_2 in the cavity mouths are almost in phase (if $\gamma_2 << 1$) and have amplitudes such that the volume displacements $A_1 Z_1$ and $A_2 Z_2$ are almost equal. This gives rise to a corresponding minimum of p_1, which is seen from (2.39) to be proportional to γ_2. If there were no damping at all in the lower opening, Z_1 and Z_2 would be exactly in phase at this frequency, giving $p_1 = 0$. This explains the trend shown in Figure 10, where the predicted maximum pressure ratio between positions 4 and 2 is seen to be much greater for K = 3.83 than for K = 30.

It is of interest to carry out some calculations, based on this simple model, for the case examined in detail in the previous section. That is, coupled cavities with b_1 = 1 cm, b_2 = 0.5 cm, L_1 = 31.9 cm

and L_2 = 31.1 cm. The cavity volumes and opening areas are then given by

$$V_1 = 3{\cdot}273 \times 10^{-3}\,m^3, \quad V_2 = 3{\cdot}191 \times 10^{-3}\,m^3,$$
$$A_1 = 3{\cdot}142 \times 10^{-4}\,m^2, \quad A_2 = 7{\cdot}854 \times 10^{-5}\,m^2.$$

The sound speed is taken as 342.4 m/sec, corresponding to a temperature of 18°C. The effective fluid mass in each opening is found in the usual manner for Helmholtz resonators [7]. That is, we write

$$m_i = \rho A_i T_i \quad , \tag{2.40}$$

where the effective mouth thickness T_i is found from

$$T_i = \tau_i + \frac{16\, b_i}{3\pi} \quad . \tag{2.41}$$

If τ_2 is taken as 2.4 mm (ie the effective low frequency value deduced in the previous section), then equation (2.38) predicts that the minimum of p_1 occurs at 82Hz. This agrees well with experiment, as can be seen from Figure 10. (If τ_2 is taken as 6 mm, (2.38) gives a frequency of 71Hz, which is rather low). The resonant frequencies, with τ_2 = 2.4 mm, are predicted to be 62Hz and 148Hz. These values agree well with the first two measured resonant frequencies of 57Hz and 148Hz. The measured maximum value of p_2/p_1 is seen from Figure 10 to be about 13.5dB. Using this value in equation (2.39) gives $\gamma_2 = 1{\cdot}125 \times 10^{-4}$ kg/sec. The system response may now be calculated. Figure 13 shows the measured and computed ratio of lower to upper cavity pressure in the low frequency range ($\leq$ 200Hz). Agreement is seen to be good, indicating that the simple model is adequate for predicting relative sound pressure levels between cavities at low frequencies. At high frequencies the model breaks down, since the existence of higher modes of resonance is not recognised.

3. FLEXIBLE-WALLED CAVITY SYSTEM

(a) Experiment

An experimental programme is currently being carried out with the object of investigating flow excited resonance in cavities having flexible walls, with water as the fluid medium. The essential features of the model used in these experiments are sketched in Figure 5 below.

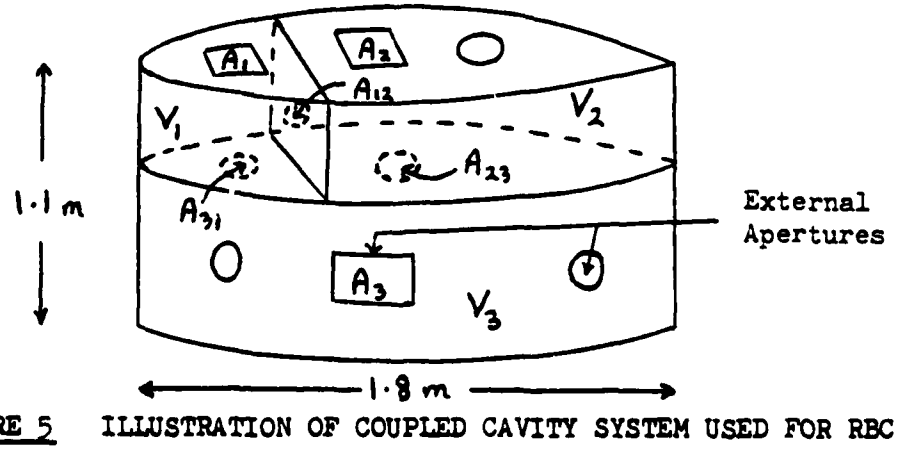

FIGURE 5 ILLUSTRATION OF COUPLED CAVITY SYSTEM USED FOR RBC TESTS

The model is fabricated from 6mm thick steel plate and contains three cavities, separated by internal bulkheads as shown in the diagram. The volumes of the cavities are given approximately by $V_1 = 0.045\ m^3$, $V_2 = 0.14\ m^3$, $V_3 = 0.41\ m^3$. The three volumes are thus approximately in the ratio $V_1:V_2:V_3 = 1:3:9$. Circular apertures A_{ij} are shown connecting the cavities. The subscripts i and j are chosen so that A_{ij} is an opening connecting V_i and V_j. A_{12} and A_{31} are 5 cm in diameter, while the diameter of A_{23} is 10 cm. Each of these apertures can be blanked off by a covering plate if required in order to reduce the coupling between the cavities. It is of course not possible to isolate the cavities from each other completely because the internal plating is not perfectly rigid. Furthermore there are a number of small holes in the horizontal internal plate which cannot be blanked off. These are necessary to ensure complete flooding of the model when it is immersed in water. In addition to the internal apertures A_{ij} there are a number of external openings connecting the cavities with the exterior. Three of these are labelled as A_1, A_2 and A_3 in Figure 5. (There are in fact six external openings in the model, one connecting with V_1, two with V_2 and three with V_3, as shown. However, for the purpose of the present study it is not necessary to consider the details of all six openings, so only three are labelled here, one to each volume). The area of each opening can be varied by the insertion of various plates, which can be used to block off the whole or part of any opening.

The cross-sectional shape of the structure is a NACA 0024 profile, which is a suitable shape for towing in the Rotating Beam Channel (RBC) at Teddington. Towing speeds of up to 12m/sec are employed in the experiment, in which resonances of the system are excited via flow over the external apertures. The internal sound spectra are measured by three hydrophones, one in each cavity. It is also possible to measure vibrations of the cavity walls by means of three accelerometers, which can be fixed magnetically to various parts of the plating. No measurements have been made of sound spectra outside the model since the RBC, being an annular channel with concrete walls, does not readily lend itself to measurements of radiated noise.

Various resonant frequencies of the system can be excited by varying the towing speed and the sizes of the external apertures. In all cases the resonant frequencies observed are less than 200Hz, and most are between 10 and 100Hz. The full details of the system response as a function of towing speed, for various configurations of the external openings, are to be described in a later report. In this study we are concerned with only one aspect of the response, namely the relative SPLs between the three cavities in the model. As in the case of the rigid walled cavities, a description is given of the theoretical model of the system before proceeding to a discussion of experimental results.

(b) Theoretical Model

In view of the complexity of the structure shown in Figure 5 a rigorous solution of the wave equation is not feasible without recourse to a sophisticated technique such as the Finite Element method. Such an

approach is not considered justified in the present case since the aim of this study is to produce the simplest theory capable of describing the essential features of the system and of predicting the general trends observed. High accuracy is not required. The success of the simplified model of two coupled cavities with rigid walls, presented in Section 2(d), leads to the expectation that a similar approach should successfully predict the main features of a more complex system with flexible walls, provided always that the acoustic wavelength λ is large compared to the physical dimensions of the system. In the present case all the resonances excited by the flow are less than 200Hz, giving $\lambda > 7.3$ m. The largest dimension of the model is 1.8 m. Hence the acoustic pressure must be approximately in phase throughout any individual cavity in the frequency range of interest. The essential differences between the model described here and that of Section 2(d) are the inclusion of wall flexibility and the neglect of viscous damping. The latter has been shown not to be an important factor in determining the relative SPL between resonating coupled cavities.

The notation used in the theory is defined below.

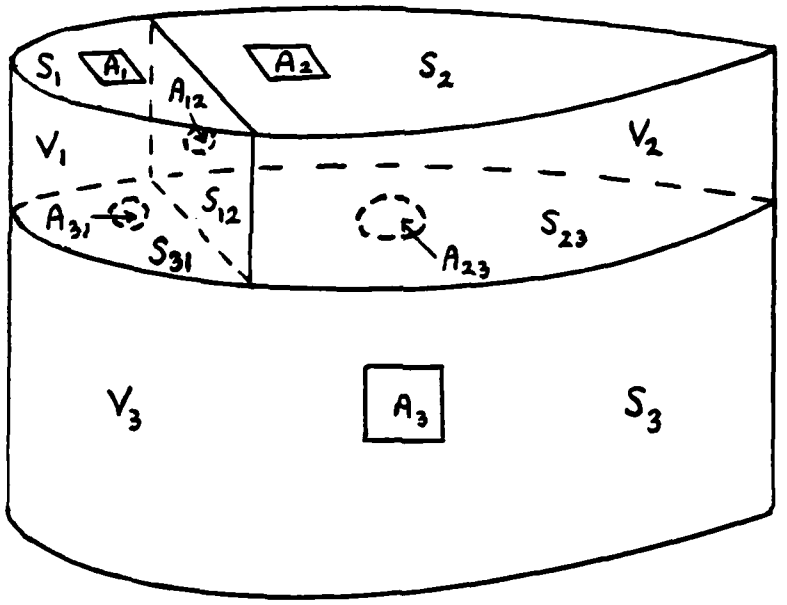

FIGURE 6 ILLUSTRATION OF NOTATION FOR THEORETICAL MODEL OF COUPLED CAVITIES

c_w = sound speed in water
c_a = sound speed in air
ρ_w = density of water
ρ_a = density of air
V_i = i^{th} cavity (i = 1,2,3). Also used for numerical value of the volume of i^{th} cavity
A_i = area of external opening
S_i = area of plating external to V_i
p_i = acoustic pressure in V_i
δ_i = volume fraction of air in V_i
m_i = effective mass of oscillating fluid in aperture A_i
K_i = stiffness of plating of area S_i

M_i = effective mass of plating of area S_i
F_i = external force applied to fluid in area A_i
x_i = displacement of mass m_i
y_i = displacement of plate S_i
A_{ij} = area of internal opening connecting V_i and V_j
S_{ij} = area of plating between V_i and V_j
m_{ij} = effective fluid mass in opening A_{ij}
K_{ij} = stiffness of plating of area S_{ij}
M_{ij} = effective mass of plating of area S_{ij}
x_{ij} = displacement of mass m_{ij}
y_{ij} = displacement of plate S_{ij}

The sign convention is as follows: p_i is positive for an increase in pressure, and x_i, y_i are positive for an outward displacement. x_{ij} and y_{ij} are positive for a displacement from volume i towards volume j and F_i is positive for a force tending to displace m_i outwards.

Each area of plating is represented as a simple one-dimensional oscillator having only one resonant frequency. This is of course a great simplification of the full equations governing the plate motions, particularly since the external plating areas S_1, S_2 and S_3 are each comprised of both curved and flat portions having distinct oscillatory characteristics. However, if the natural frequencies of the plating are significantly greater than the resonant frequencies of the overall system (as is the case here), then the system response is stiffness-dominated at low frequencies and it is not important to determine accurately the vibrational characteristics of each separate part of the plating. This point is discussed further in Section 3(c).

The equations of motion of the masses m_i and m_{ij} may now be written as

$$m_i \ddot{x}_i = A_i p_i + F_i \,, (i = 1, 2, 3) \,, \tag{3.1}$$

$$m_{ij} \ddot{x}_{ij} = A_{ij} (p_i - p_j) \,, \begin{pmatrix} i = 1,2,3 \\ j = 2,3,1 \end{pmatrix} \,, \tag{3.2}$$

and the equations of motion of the plating are given by

$$M_i \ddot{y}_i + K_i y_i = S_i p_i \,, \tag{3.3}$$

$$M_{ij} \ddot{y}_{ij} + K_{ij} y_{ij} = S_{ij} (p_i - p_j) \,. \tag{3.4}$$

Because of the complexity of the structure it has not been possible to estimate added mass effects, so the induced pressure loading on the outer surface of the plating has been ignored. Hence the RHS of equation (3.3) contains only the internal pressure p_i.

The above is a system of 12 equations in the 15 variables x_i, x_{ij}, y_i, y_{ij} and p_i. It remains to express the acoustic pressures p_i in terms of the displacements of the plating and fluid masses. In the following analysis, allowance has been made for the presence of air in the cavities. (In all the experiments conducted so far the cavities have been

completely water filled, but future work may incorporate the introduction of known amounts of air into the system.) Let δ_i be the volume fraction of air in V_i at the ambient pressure, so that the respective volumes of air and water in V_i are V_a $(= \delta_i V_i)$ and V_w $(= \overline{1 - \delta_i} V_i)$. Now let the total volume increase by an amount ΔV_i under the action of the external forces, with corresponding increments ΔV_a and ΔV_w in the volumes of air and water.

$$\therefore \quad \Delta V_a + \Delta V_w = \Delta V_i \ . \tag{3.5}$$

Now the masses of air and water remain constant, so we have $\Delta(\rho_a V_a) = 0$.

$$\text{Thus} \quad \rho_a \Delta V_a + V_a \Delta \rho_a = 0 \ , \tag{3.6}$$

with a similar expression for the water mass.

$$\text{That is,} \quad \frac{V_a}{\rho_a} \Delta \rho_a + \frac{V_w}{\rho_w} \Delta \rho_w = -\Delta V_i \ . \tag{3.7}$$

The pressure increment p_i is related to the density changes $\Delta \rho_a$ and $\Delta \rho_w$ by the equations

$$p_i = c_a^2 \Delta \rho_a = c_w^2 \Delta \rho_w \ ,$$

where isentropic expansion has been assumed. Hence (3.7) gives

$$\frac{V_a}{\rho_a} \frac{p_i}{c_a^2} + \frac{V_w}{\rho_w} \frac{p_i}{c_w^2} = -\Delta V_i \ , \tag{3.8}$$

which is written in terms of δ_i as

$$V_i \rho_i \left[\frac{\delta_i}{\rho_a c_a^2} + \frac{1 - \delta_i}{\rho_w c_w^2} \right] = -\Delta V_i \ . \tag{3.9}$$

The volume increments ΔV_i are written in terms of the displacements x_i, y_i etc. That is,

$$\Delta V_1 = A_1 x_1 + A_{12} x_{12} - A_{31} x_{31} + S_1 y_1 + S_{12} y_{12} - S_{31} y_{31} \ , \tag{3.10}$$

with similar expressions for ΔV_2 and ΔV_3. This completes the system of 15 equations.

It is now assumed, in the usual manner, that all quantities vary as $e^{i\omega t}$, where ω is the radian frequency of the forcing terms $F_i(t)$. Substituting $e^{i\omega t}$ for the time dependence in equations (3.1) to (3.4) gives

$$\begin{aligned} x_i &= -(A_i \rho_i + F_i)/m_i \omega^2 \ , \\ x_{ij} &= -A_{ij}(\rho_i - \rho_j)/m_{ij} \omega^2 \ , \\ y_i &= S_i \rho_i / (K_i - M_i \omega^2) \ , \\ y_{ij} &= S_{ij}(\rho_i - \rho_j)/(K_{ij} - M_{ij} \omega^2) \ . \end{aligned} \tag{3.11}$$

When these expressions are substituted into (3.9) the acoustic pressures in the cavities can be determined as functions of frequency in terms of the amplitudes and phases of the forcing terms by solving the resulting system of three linear equations. Phase differences between the F_j can be allowed for by the inclusion of factors $e^{i\phi_j}$, where ϕ_j is a phase angle.

The effective masses m_i and m_{ij} are found using the usual approximation for Helmholtz resonators [7]. That is,

$$m_i = \rho_w A_i T_i \quad , \quad m_{ij} = \rho_w A_{ij} T_{ij} \quad , \tag{3.12}$$

where T_i (or T_{ij}) is the effective thickness of an opening. If the geometric thickness is small in relation to the diameter, T_i is given by

$$T_i \simeq 0.96\sqrt{A_i} \quad . \tag{3.13}$$

This equation is equivalent to (2.41) in the case of a circular opening. It is strictly meant to apply only when there is no external flow. The presence of a non-zero flow past an external opening effectively reduces the reactance at the opening [8], so that m_i would be smaller than the value found from equations (3.12) and (3.13). However, no attempt has been made here to model the relationship between flow speed and effective fluid mass.

At the resonant frequencies of the system, the acoustic pressures, found from equations (3.9) to (3.11), become infinite, since no damping has been included. However, the ratio of acoustic pressures between cavities remains finite at resonance, and it is these pressure ratios with which the present theory is principally concerned. The following section contains a discussion of some of the experimental results obtained to date, together with corresponding theoretical predictions.

(c) Comparison of Theory and Experiment

Since the external excitation of the RBC model is provided by water flow over the external openings rather than a variable frequency driving wave, it is not possible to measure frequency responses in the same manner as for the rigid walled cavity system. Resonant frequencies excited by the flow appear as well-defined lines in the acoustic spectrum, having levels well above the background. At frequencies away from resonance the high level of background noise makes accurate measurement impossible, so in this section attention is concentrated on the system response at resonance, which is in any event the situation of greatest practical interest.

One of the most noticeable features of the experimental results was the fact that very large differences in SPL were sometimes observed between adjoining cavities, even though the internal apertures A_{ij} were uncovered, thus providing a direct fluid path between any two cavities of the system. For example, in the case $A_1 = A_3 = 0$, $A_2 = 169$ cm^2 (see Figure 6), a resonant frequency of about 30Hz was excited for towing speeds of 7 m/sec

and above. (The resonant frequency was speed dependent to some extent, varying from 26Hz at 7 m/sec to 32Hz at 11 m/sec because of the decreasing reactance of the opening.) The highest SPL at this frequency was recorded in V_2. This level was about 6dB above the level in V_1, but as much as 40dB above the level in V_3. The theory described in the preceeding section should be capable of predicting this type of behaviour provided that the essential features of the system have been included in the model and that appropriate estimates are made of the effective masses and stiffnesses of the various parts of the structure. Impact response tests in air, in which the vibrational response of the structure was recorded after striking the model, indicate a lowest plate structural resonant frequency of about 170Hz. When the model is immersed in water the plate resonances are subjected to two opposing factors. These are (a) the effect of the external fluid, which is equivalent to an added mass and tends to reduce the structural frequencies, and (b) the effect of the internal fluid, which for low frequencies acts like a massless spring and therefore tends to increase the structural frequencies by means of "added stiffness". Approximate calculations indicate that, for this model, the added stiffness is the dominant factor, so that the structural frequencies in water should be greater than those measured in air, at least for the lowest modes. It is therefore expected that the structural response below 100Hz is dominated by stiffness and is virtually independent of mass. That is, it is not essential to choose the effective masses M_i and M_{ij} accurately in order to obtain a satisfactory model of the low-frequency response. The values of M_i and M_{ij} were therefore specified simply as the static masses of the relevant areas of plating, calculated for steel of 6 mm thickness. The numerical values used are as follows, with all masses in kg and surface areas in m^2.

$$S_1 = 0.49, \quad S_2 = 1.44, \quad S_3 = 3.36, \quad S_{12} = 0.16, \quad S_{23} = 0.40, \quad S_{31} = 0.3$$

$$M_1 = 23.3, \quad M_2 = 67.9, \quad M_3 = 158.4, \quad M_{12} = 7.4, \quad M_{23} = 18.9, \quad M_{31} = 6.1.$$

It remains to specify the effective stiffnesses K_i and K_{ij}. These were chosen on the basis of experimentally determined resonant frequencies using the following procedure. With the internal apertures A_{ij} blanked off, the model was towed at a range of speeds for three separate geometric configurations, defined by

(i) $A_1 = 64\ cm^2, \quad A_2 = A_3 = 0$

(ii) $A_2 = 169\ cm^2, \quad A_3 = A_1 = 0$

(iii) $A_3 = 484\ cm^2, \quad A_1 = A_2 = 0.$

The lowest resonant frequency of the system was measured in each case, and was assumed to be a Helmholtz resonance of the appropriate cavity. The mean measured frequencies were approximately 56Hz, 25Hz and 11Hz for configurations (i), (ii) and (iii) respectively. The stiffnesses of the cavity boundaries were then chosen in order to force agreement between measured and predicted values for the above configurations. The resulting values of K_i and K_{ij} (in kg/sec^2) are shown below.

$$K_1 = 4 \times 10^8, \quad K_2 = 4 \times 10^8, \quad K_3 = 2.4 \times 10^8$$

$$K_{12} = 10^{10}, \quad K_{23} = 3 \times 10^8, \quad K_{31} = 4 \times 10^8.$$

These values of plate stiffness were then held constant for subsequent calculations. The test of the validity of the theory lies in its ability

to predict resonant frequencies and relative sound pressure levels for the fully coupled system, when the internal blanking plates are removed. (ie $A_{i,j} \neq 0$). Theoretical results for this case, with a number of different external apertures, are tabulated below. For these calculations the mass of fluid at the external opening was found from (3.12) and (3.13).

Area of opening (cm^2)			Resonant frequency (Hz)		
A_1	A_2	A_3	f_1	f_2	f_3
64	0	0	5.5	24	81
0	169	0	6.0	33	60
0	0	113	7.8	24	60
0	0	484	11	24	60

TABLE 5 Calculated Resonant Frequencies of Coupled Cavity System.

The theory is not capable of predicting resonant modes beyond the third, since the model contains only three degrees of freedom, corresponding to the three coupled cavities. Each mode corresponds to a different combination of phase relationships between the oscillatory motions in the various openings (ie in phase or out of phase). The system should therefore be regarded as a generalised Helmholtz resonator, having three modes of vibration. A system with n cavities would have n modes. There are, in general, no simple numerical relationships among the natural frequencies for any given configuration.

The frequencies shown in Table 5 above are very different from those predicted for a rigid walled cavity system. For example, in the case $A_1 = 64$ cm^2, a calculation in which the flexibility of the plating is ignored produces resonant frequencies of 65, 250 and 468Hz. Representation of wall flexibility is therefore essential in a structure such as this, with water as the fluid medium. The effects of non-rigidity of the walls would of course be much less pronounced in air.

We consider now the measured resonant frequencies of the coupled system, and compare them with the predictions of Table 5. In the case $A_1 = 64$ cm^2 a strong resonance was excited in the range 79-88Hz. This appears to correspond to the predicted third mode at 81Hz. (It has already been mentioned that the observed resonant frequencies varied somewhat with towing speed. The figures of 79Hz and 88Hz represent the frequency limits of the observed resonance.) In this case no lower mode was excited, but in the case $A_2 = 169$ cm^2 a resonance was excited in the frequency range 26-32Hz. This corresponds closely with the predicted second mode at 33Hz. In only one case was the lowest mode excited strongly. This was with $A_3 = 484$ cm^2, when two resonances were observed, in the ranges 11-16Hz and 21-24Hz. For this configuration the predicted frequencies are 11, 24 and 60Hz. The third mode was not observed. For a somewhat lower value of A_3 (113 cm^2) only the second mode was excited, at 20-28Hz. The predicted second resonant frequency is 24Hz for this case. Overall agreement between predicted and measured resonant frequencies is therefore seen to be quite good, bearing in mind the simplicity of the theoretical model.

The resonant frequencies shown in Table 5 were all found using equations (3.12) and (3.13) for the mass of fluid at the external opening,

but this is known to be inadequate in the presence of a flow past the opening since the effective mass decreases with increasing flow speed [8]. This effect is simulated simply by carrying out a series of calculations in which m_i is varied, all other parameters being held constant. For example, in the case $A_1 = 64\ cm^2$, a reduction in m_1 from 0.5 kg (the value given by (3.12)) to 0.35 kg, leads to an increase in the predicted resonant frequency of the third mode from 81Hz to 88Hz. The observed variation was 79-88Hz. The correct trend is therefore predicted. However, no attempt has been made to formulate a relationship between m_i and towing speed. The figure of 0.35 kg for m_1 is quoted simply because it produces a resonant frequency of 88Hz, and not from any independent functional relationship between speed and effective mass. The same trend is observed with most of the other resonances (ie frequency increasing as mass is reduced), but the sensitivity of a resonant frequency to variations in the mass at the opening is of course dependent on the particular geometry under consideration.

Agreement between measured and predicted sound pressure levels in the three cavities is less consistent than the agreement between resonant frequencies, although very good correlation is obtained in some cases. Consider, for example, the case $A_1 = 64\ cm^2$, $A_2 = A_3 = 0$. Writing I_j for the SPL in volume V_j, the mean predicted relative SPL values at the third resonant frequency are given by

$$I_1 - I_2 = 31dB, \quad I_1 - I_3 = 53dB.$$

These values are virtually independent of small variations in resonant frequency, changing by no more than $\pm$ 1dB from the mean values as f_3 increases from 81 to 88Hz. Measured values for this case are as follows:

f_3 (Hz)	$I_1 - I_2$ (dB)	$I_1 - I_3$ (dB)
81	38	54
85	35	52
87	30	(not measured)

The good agreement between measured and predicted values gives confidence that the modes of oscillation measured are indeed those modelled by the simple theory presented here. This degree of agreement is not attained in all cases. However, in view of the approximations made the model is considered to give a reasonable representation of the system response at low frequencies.

It can be seen that the relative SPL between adjoining cavities can be very large. The value of over 50dB recorded above for $I_1 - I_3$, is not untypical. These large differences occur even though the acoustic wavelength is much greater than the model dimensions, and even when there is a direct coupling between the volumes via the internal aperture. In the above case the highest SPL occurs in V_1, which is the volume directly adjoining opening A_1 where the excitation occurs. However, this is not

always so. Consider, for example, the case $A_3 = 113\ cm^2$, $A_1 = A_2 = 0$. At a towing speed of 10 m/sec a 28Hz resonance is excited, with measured acoustic pressure differences given by $I_3 - I_1 = -1.7dB$, $I_3 - I_2 = -7.4dB$. Thus the lowest SPL occurs in V_3 even though this is the cavity to which the excitation is applied.

An example of the predicted variation in relative sound pressure levels with frequency is shown in Figure 14, for the case $A_2 = 169\ cm^2$. The graph covers the range 20 to 50Hz, which includes the observed resonance in the range 26-32Hz. Experimental values of $I_1 - I_2$ and $I_2 - I_3$ are shown on the same graph. Agreement is moderately good except when the towing speed reaches 10 m/sec, at which point $I_2 - I_3$ suddenly increases from about 15dB to 40dB due to a sudden reduction in I_3. This phenomenon, which is not accounted for by the simple theoretical model, will be discussed in a future report together with other aspects of the experimental work. The simple theory cannot be expected to cope with all the observed features of flow excited resonance in a complex structure. It has, however, proved adequate to explain some of the interesting features associated with a system of coupled cavities.

4. CONCLUSIONS

Theoretical models have been developed to describe the behaviour of coupled cavities, and the predictions of the theories have been compared with experimental results. It has been shown that viscosity is unlikely to affect the acoustic transmission between coupled resonating cavities except in cases of very small openings (possibly of the order of 1 mm diameter) whose length is large in relation to the size of the opening. Although this conclusion has been drawn on the basis of results for hard walled cylindrical cavities in air, it is believed to be valid for more general configurations in air or water.

The wave equation solution for cylindrical cavities is found to agree well with experiment and is valid for a wide range of frequencies, but suffers from the restriction of being applicable only to the simple cylindrical geometry used in the experiments. A simpler theory for two coupled hard-walled cavities (not necessarily cylindrical) is found to give equally good predictions of sound transmission between the cavities, but this simple model is valid only for low frequencies.

In order to describe the acoustic behaviour of the system of three coupled cavities in water for low frequencies, the simplified theoretical approach was extended and generalised to include wall flexibility. Good agreement is again obtained between measured and predicted natural frequencies of the system, and the theory is found to reproduce fairly well some of the measured differences in SPL between adjoining cavities. The inclusion of wall flexibility is crucial to the success of this theory, since the effect of the wall properties on the system response is particularly marked in water.

A number of interesting features have arisen from the experiments with the three-cavity model in water. Firstly, it has been found that very large differences in sound pressure level can occur between adjacent coupled cavities even when there is a direct fluid path between the cavities and when the acoustic wavelength is large in relation to the physical dimensions of the structure. Secondly, it has been shown that the highest acoustic pressure does not necessarily occur in the cavity adjoining the opening where the excitation of resonance occurs via the external flow. These effects do not rely for their existence upon the non-rigidity of the cavity structure or upon the fluid medium being water, but it is in the experiments carried out in water that the largest effects were observed. Differences of over 50dB in the

sound pressure level at resonance have been observed between adjoining cavities. A much more accurate representation of the RBC model could be made using more sophisticated techniques such as finite elements. However, the time and effort involved in doing this was not felt to be justified for the purpose of the present theoretical study, which was aimed at reproducing the gross features of the system in order to provide an explanation of the observed behaviour.

ACKNOWLEDGEMENTS

Grateful thanks are due to Mr G P E Barlow, Mrs L J Coley and Mr P J Rowland for performing the experimental work described in this report, and to Mrs Coley for carrying out the programming and computations associated with the theory described in Section 3.

Dr A J ROBINS (PSO)

AJR/APG

REFERENCES

1. ROBINS, A.J. A Theoretical and Experimental Study of Flow Induced Cavity Resonance. AMTE(N)R79102, August 1979

2. FAHMY, M.S.Y. Acoustic Resonances of Interconnected Cavities. ISVR Contract Report No 79/8, June 1979

3. RSCHEVKIN, S.N. A Course of Lectures on the Theory of Sound. Pergamon Press, 1963

4. MORSE, P.M. and INGARD, U. Theoretical Acoustics. McGraw-Hill, 1968

5. SNEDDON, I.N. Fourier Transforms. McGraw-Hill, 1951

6. HERSH, A.S. and WALKER, B. Fluid Mechanical Model of the Helmholtz Resonator. NASA CR-2904, September 1977

7. MALECKI, I. Physical Foundations of Technical Acoustics. Pergamon Press, 1969

8. HERSH, A.S. and WALKER, B. Effect of Grazing Flow on the Acoustic Impedance of Helmholtz Resonators consisting of Single and Clustered Orifices. NASA CR-3177, 1979

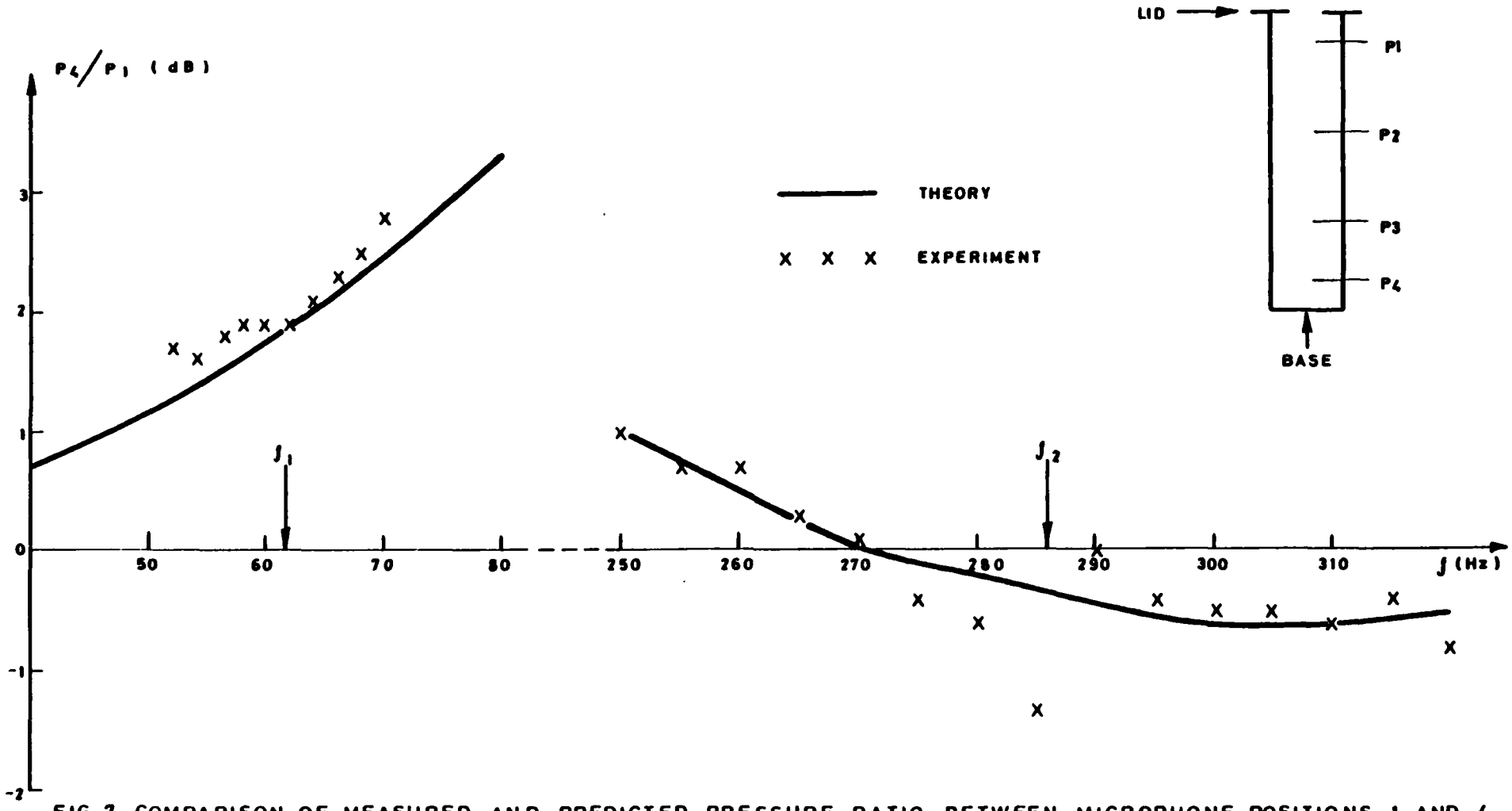

FIG. 7 COMPARISON OF MEASURED AND PREDICTED PRESSURE RATIO BETWEEN MICROPHONE POSITIONS 1 AND 4

CAVITY LENGTH = 63·6cm OPENING RADIUS = 0·75 cm

(continued overleaf)

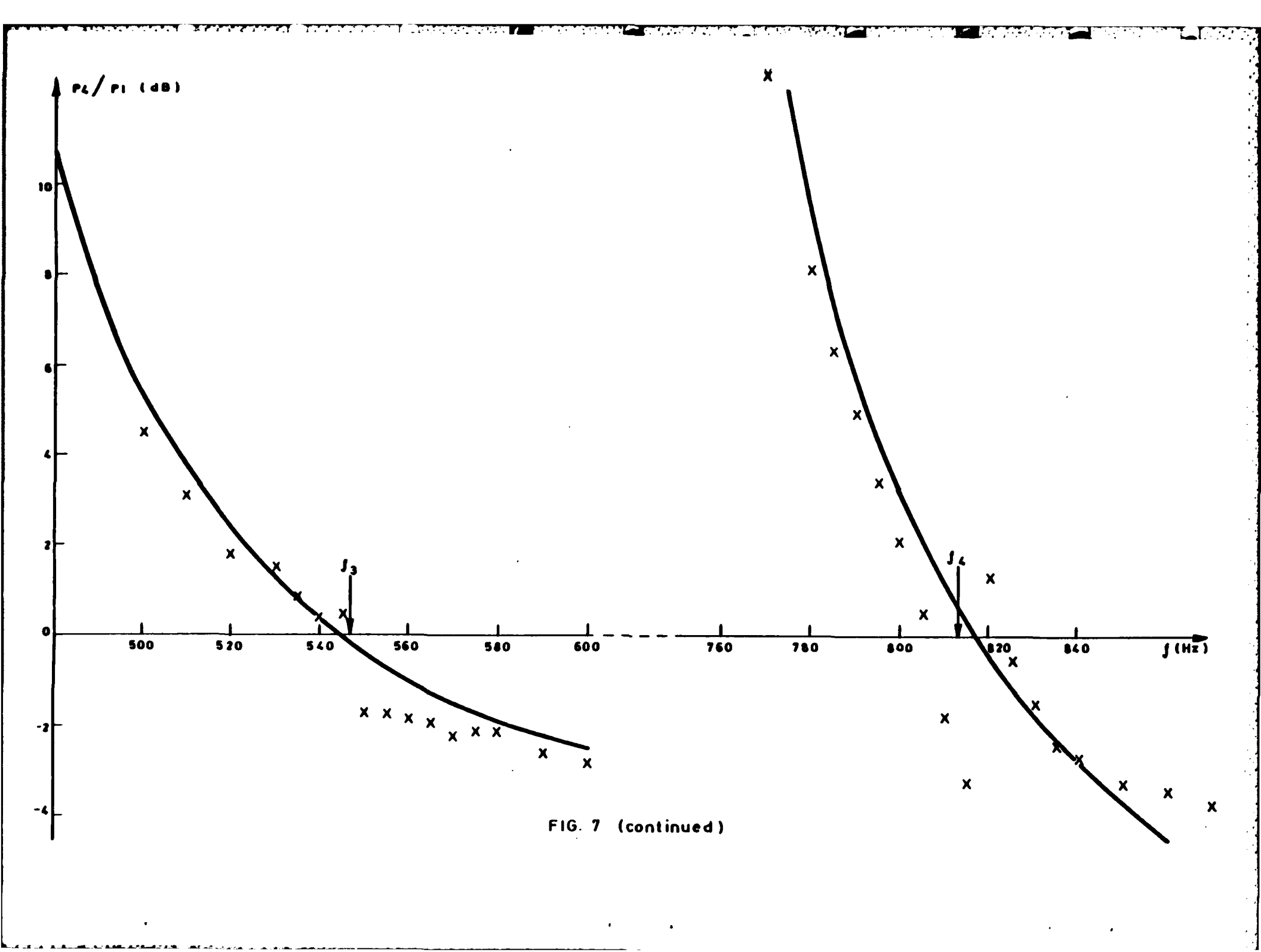

FIG. 7 (continued)

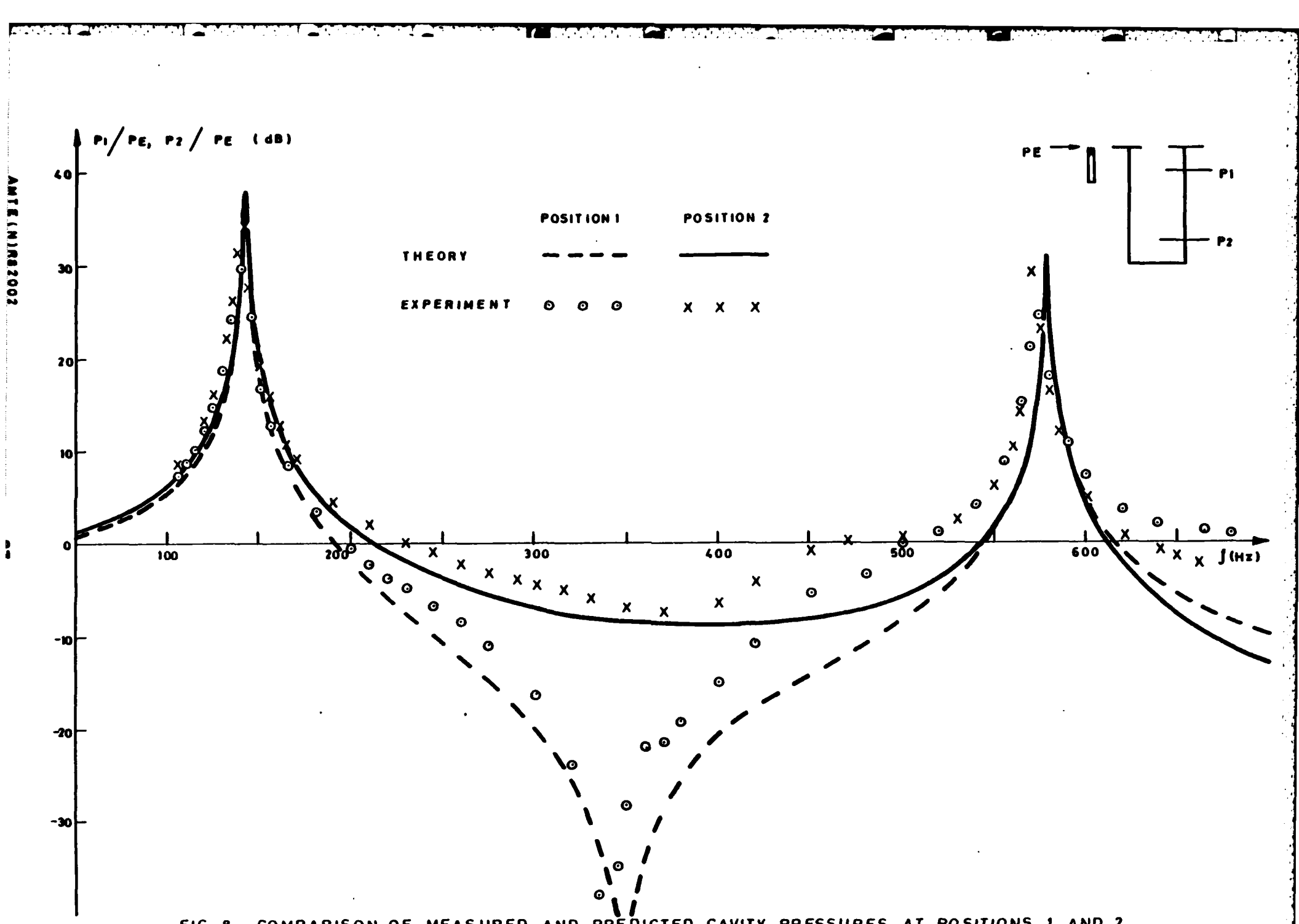

FIG. 8 COMPARISON OF MEASURED AND PREDICTED CAVITY PRESSURES AT POSITIONS 1 AND 2

CAVITY LENGTH = 32·0 cm OPENING RADIUS = 1·5 cm K = 3·46

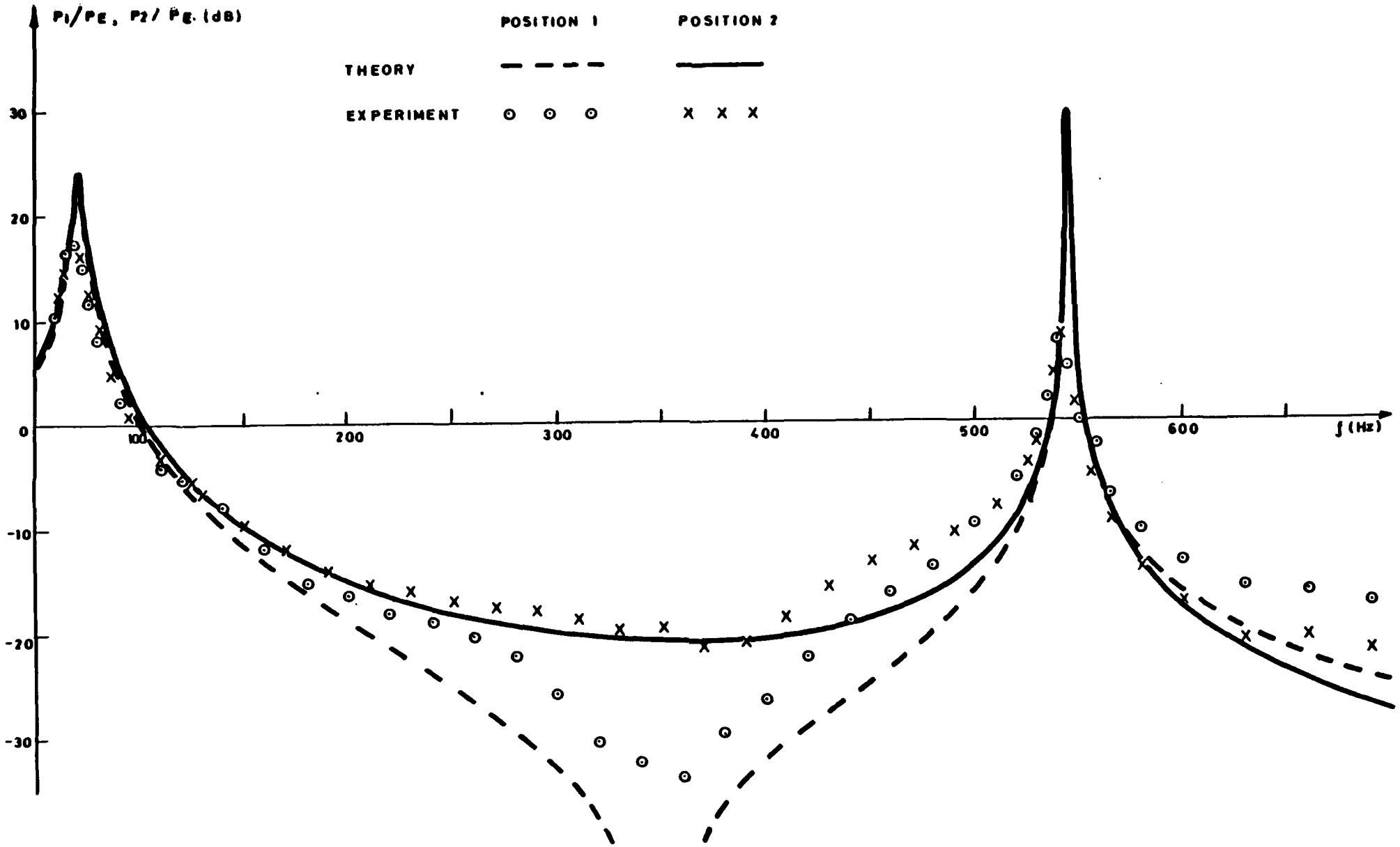

FIG. 9 COMPARISON OF MEASURED AND PREDICTED CAVITY PRESSURES

CAVITY LENGTH = 32·0cm OPENING RADIUS = 0·5cm K = 4·52

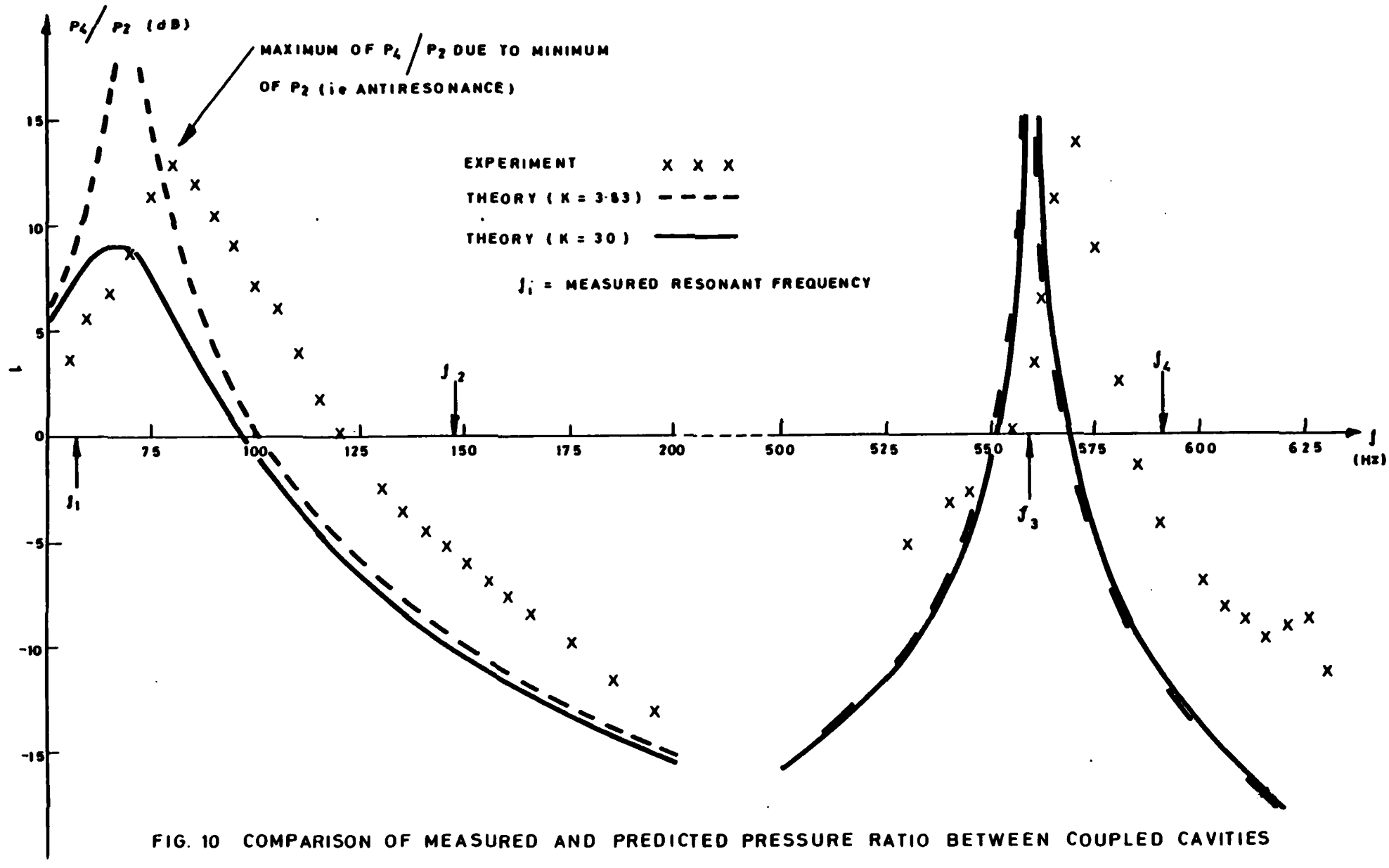

FIG. 10 COMPARISON OF MEASURED AND PREDICTED PRESSURE RATIO BETWEEN COUPLED CAVITIES

OPENING RADII = 1·0 cm (UPPER), 0·5 cm (LOWER)

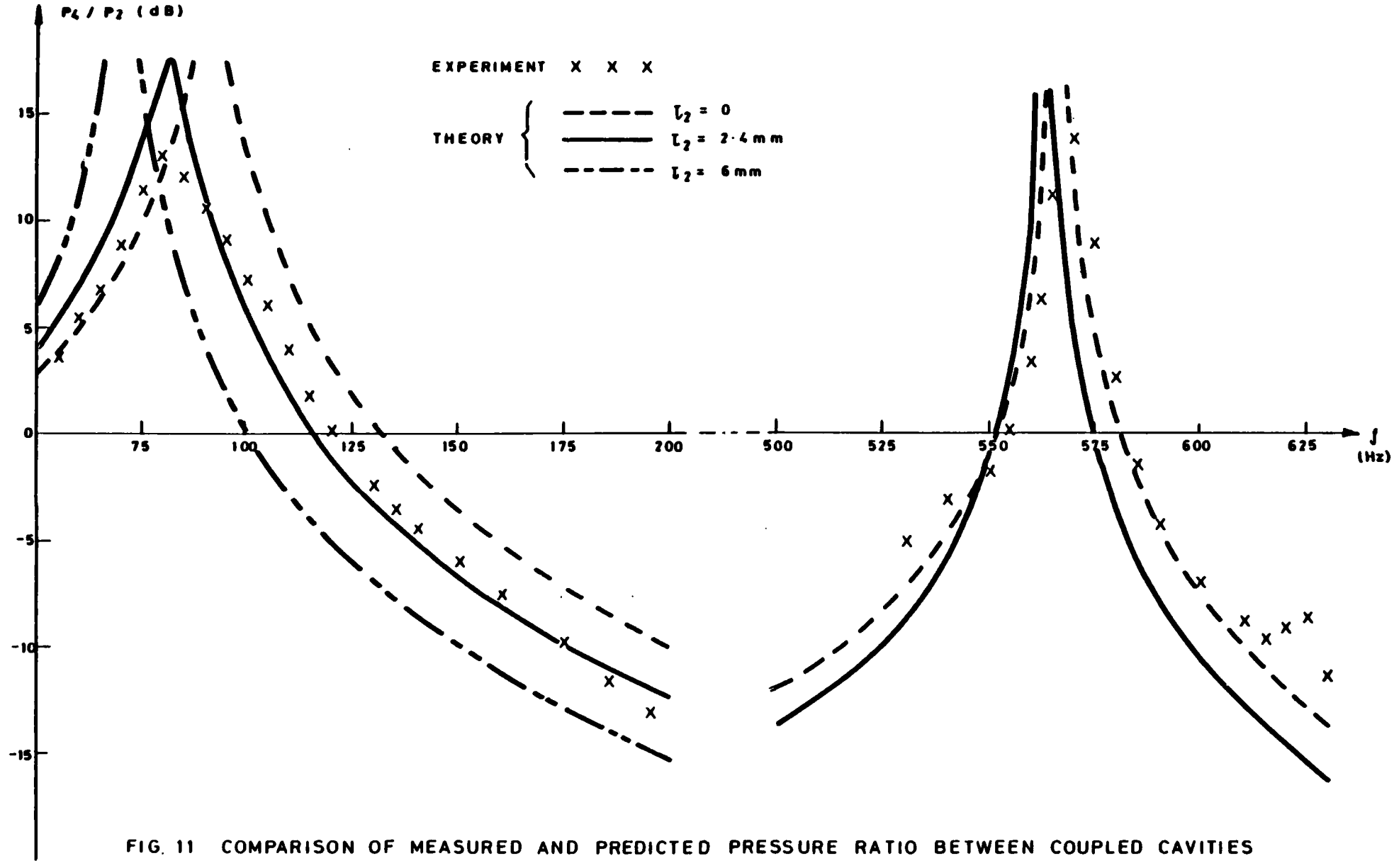

FIG. 11 COMPARISON OF MEASURED AND PREDICTED PRESSURE RATIO BETWEEN COUPLED CAVITIES

OPENING RADII = 1·0 cm (UPPER), 0·5 cm (LOWER)

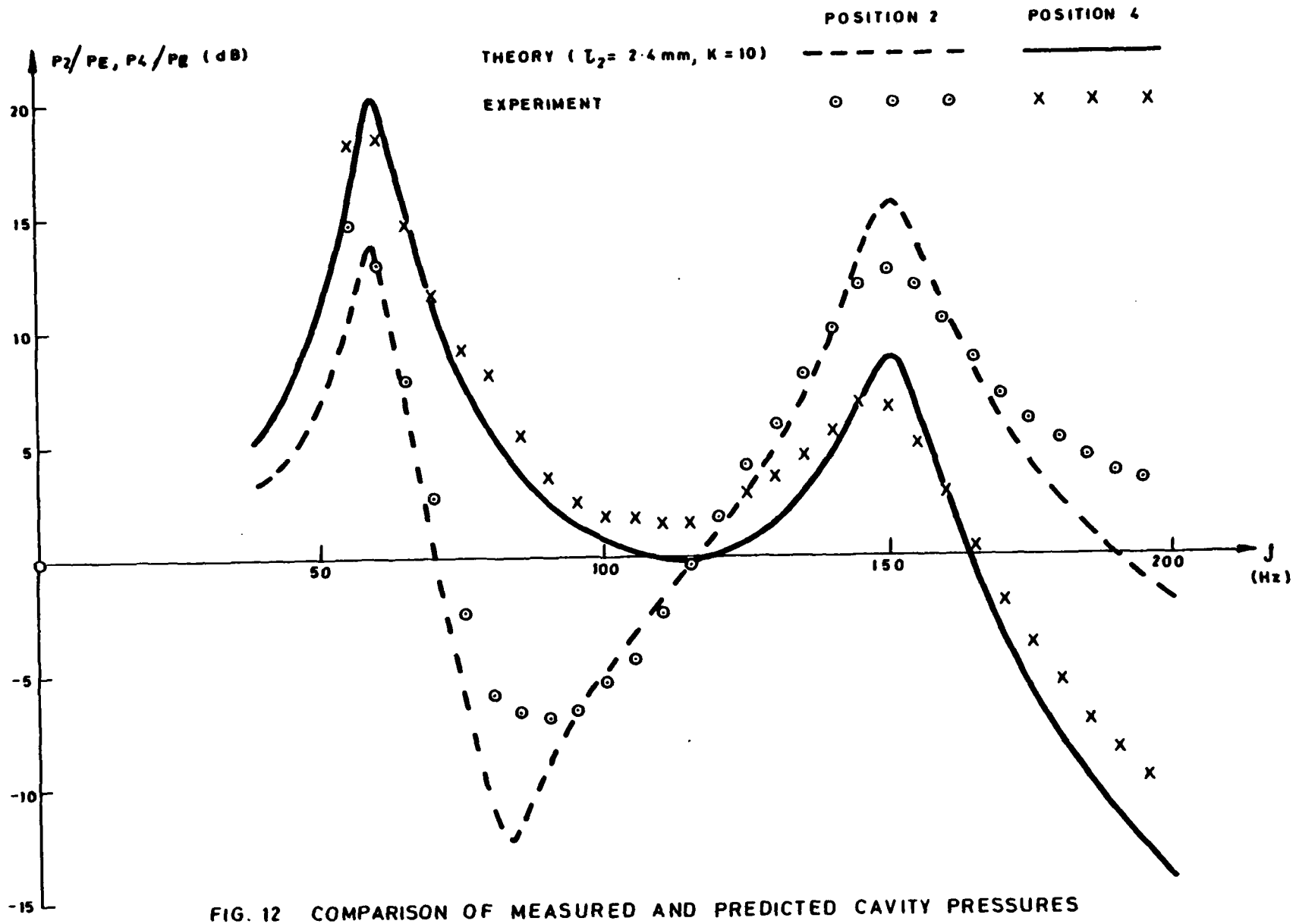

FIG. 12 COMPARISON OF MEASURED AND PREDICTED CAVITY PRESSURES FOR COUPLED CAVITIES, NEAR 1st AND 2nd RESONANCES

OPENING RADII = 1·0 cm (UPPER), 0·5 cm (LOWER)

(continued overleaf)

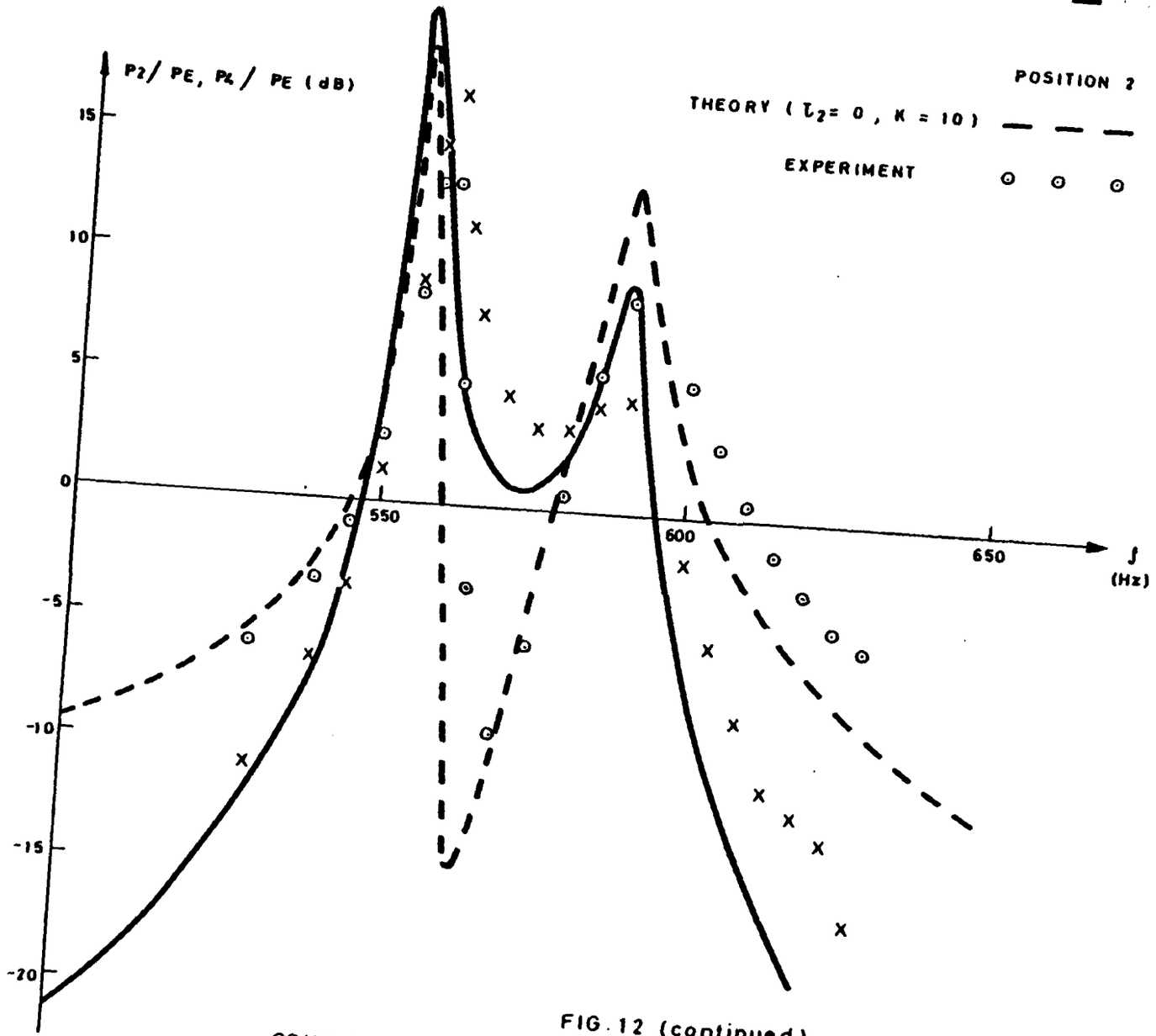

FIG. 12 (continued)
COUPLED CAVITY RESPONSE NEAR 3rd AND 4th RESONANCES

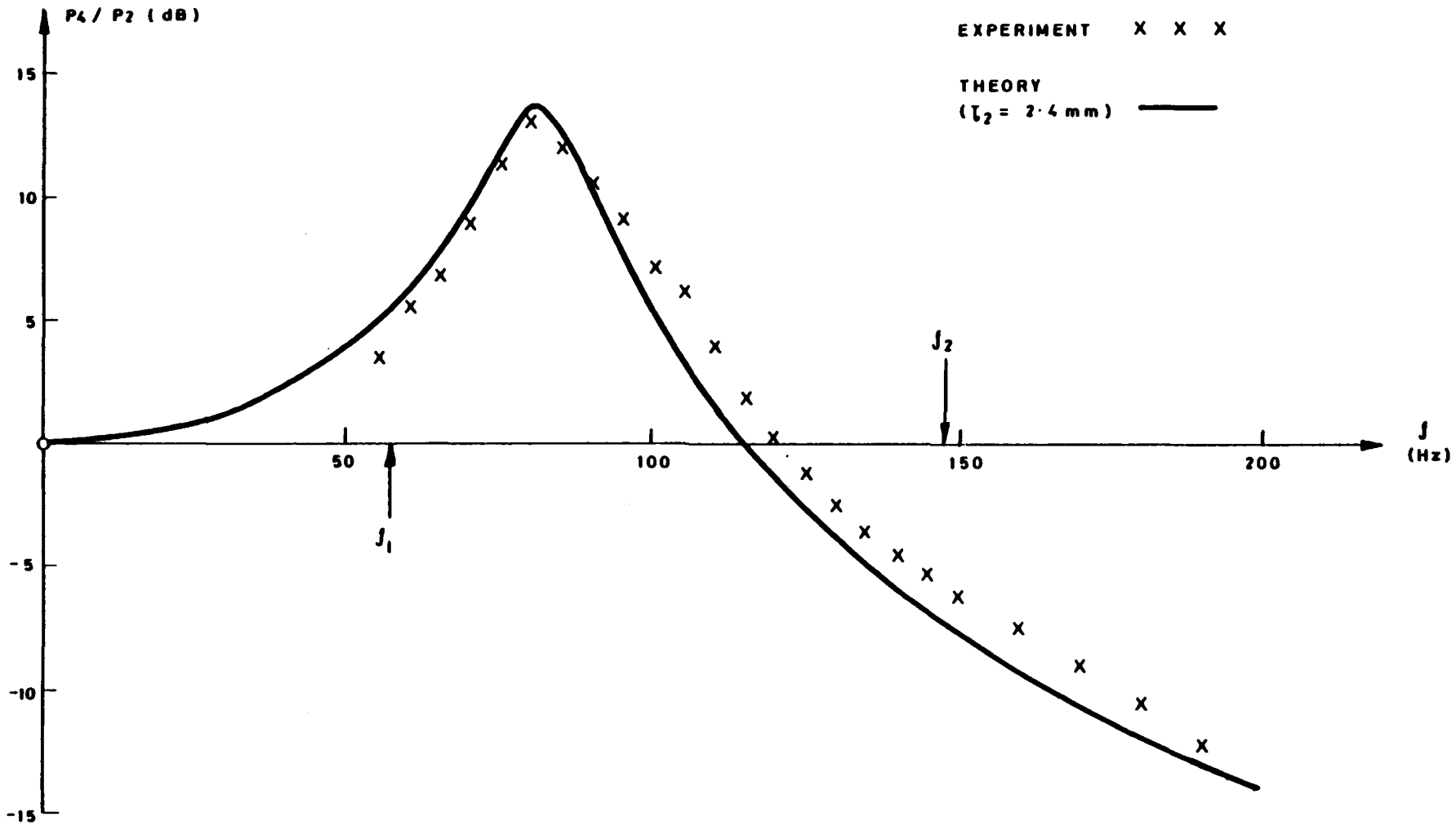

FIG. 13 COMPARISON OF MEASURED AND PREDICTED PRESSURE RATIO BETWEEN COUPLED CAVITIES USING SIMPLE THEORETICAL MODEL

$b_1 = 1\,cm,\ b_2 = 0{\cdot}5\,cm$

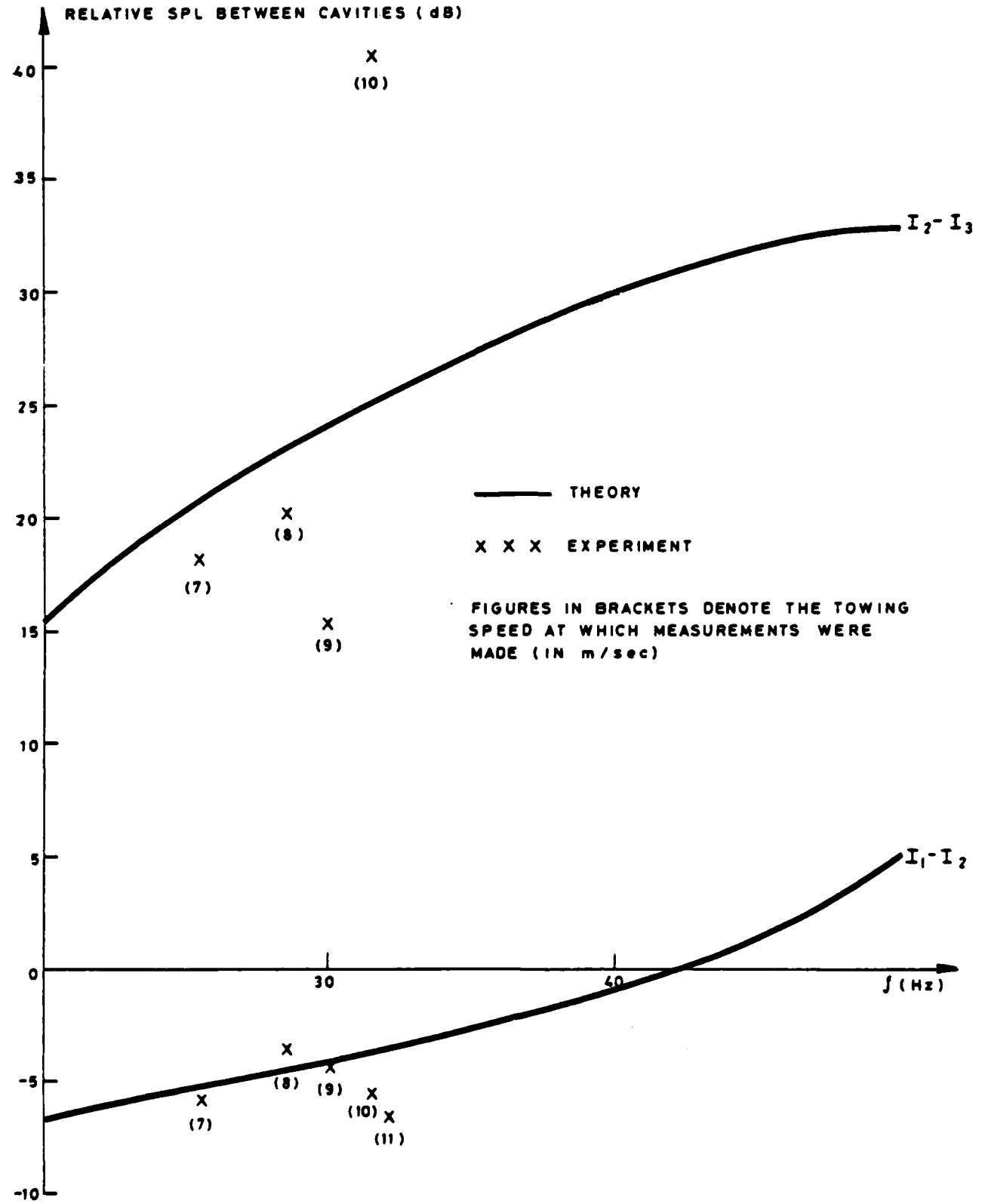

FIG. 14 PREDICTED RELATIVE SPL VALUES IN THE RANGE 20 TO 50Hz FOR $A_2 = 169 cm^2$, TOGETHER WITH EXPERIMENTAL VALUES AT RESONANCE

APPENDIX

FORMULAE FOR THE COEFFICIENTS DEFINING THE SOLUTION TO THE HELMHOLTZ EQUATION FOR COUPLED CYLINDRICAL CAVITIES

The coefficients A_n, B_n, C_n and the acoustic velocities u_1, u_2 giving the solution of equations (2.17) to (2.21), are evaluated as follows.

Define
$$\sigma_1 = \sum_{n=1}^{\infty} \frac{S_{1n}\, J_1^2\left(\frac{b_1}{a_1}\xi_n\right)}{\mu_n \xi_n^2 J_0^2(\xi_n)} ,$$

where
$$S_{1n} = \begin{cases} -\cot(\mu_n L_1/a_1) , & ka_1 \geq \xi_n \\ \coth(\mu_n L_1/a_1), & ka_1 < \xi_n \end{cases} ;$$

$$\sigma_2 = \sum_{n=1}^{\infty} \frac{S_{2n}\, J_1\left(\frac{b_1}{a_1}\xi_n\right) J_1\left(\frac{b_2}{a_1}\xi_n\right)}{\mu_n \xi_n^2 J_0^2(\xi_n)} ,$$

where
$$S_{2n} = \begin{cases} \operatorname{cosec}(\mu_n L_1/a_1) , & ka_1 \geq \xi_n \\ -\operatorname{cosech}(\mu_n L_1/a_1), & ka_1 < \xi_n \end{cases} ;$$

$$\sigma_3 = \sum_{n=1}^{\infty} \frac{a_2}{a_1} \cdot \frac{S_{3n}\, J_1^2\left(\frac{b_2}{a_2}\xi_n\right)}{\eta_n \xi_n^2 J_0^2(\xi_n)} ,$$

where
$$S_{3n} = \begin{cases} -\cot(\eta_n L_2/a_2), & ka_2 \geq \xi_n \\ \coth(\eta_n L_2/a_2), & ka_2 < \xi_n \end{cases} ;$$

and
$$\sigma_4 = \sum_{n=1}^{\infty} \frac{S_{1n}\, J_1^2\left(\frac{b_2}{a_1}\xi_n\right)}{\mu_n \xi_n^2 J_0^2(\xi_n)} .$$

The mean acoustic velocities in the upper and lower openings are then given by

$$\frac{u_1}{u_0} = \frac{-\frac{1}{4}[k(\sigma_3+\sigma_4) + \frac{1}{4}(\gamma - i\delta)]}{k^2\sigma_2^2 - [k\sigma_1 + \frac{1}{4}(\alpha - i\beta)][k(\sigma_3+\sigma_4) + \frac{1}{4}(\gamma - i\delta)]} ,$$

$$\frac{u_2}{u_0} = \frac{\frac{1}{4}\left(\frac{b_1}{b_2}\right)k\sigma_2}{k^2\sigma_2^2 - [k\sigma_1 + \frac{1}{4}(\alpha - i\beta)][k(\sigma_3+\sigma_4) + \frac{1}{4}(\gamma - i\delta)]} .$$

The coefficients A_n, B_n and C_n are defined by

$$A_n = \frac{2u_2\left(\frac{b_2}{a_1}\right)\cos\left(\frac{\mu_n L_1}{a_1}\right)J_1\left(\frac{b_2}{a_1}\xi_n\right) - 2u_1\left(\frac{b_1}{a_1}\right)J_1\left(\frac{b_1}{a_1}\xi_n\right)}{\mu_n \sin\left(\frac{\mu_n L_1}{a_1}\right)\xi_n J_0^2(\xi_n)} , \quad ka_1 \geq \xi_n$$

$$A_n = \frac{u_1\left(\frac{b_1}{a_1}\right)J_1\left(\frac{b_1}{a_1}\xi_n\right) - u_2\left(\frac{b_2}{a_1}\right)\exp\left(\frac{\mu_n L_1}{a_1}\right)J_1\left(\frac{b_2}{a_1}\xi_n\right)}{\mu_n \sinh\left(\frac{\mu_n L_1}{a_1}\right)\xi_n J_0^2(\xi_n)} , \quad ka_1 < \xi_n$$

$$B_n = \frac{2\left(\frac{b_2}{a_1}\right)u_2 J_1\left(\frac{b_2}{a_1}\xi_n\right)}{\mu_n \xi_n J_0^2(\xi_n)} , \quad ka_1 \geq \xi_n$$

$$B_n = \frac{u_1\left(\frac{b_1}{a_1}\right)J_1\left(\frac{b_1}{a_1}\xi_n\right) - u_2\left(\frac{b_2}{a_1}\right)\exp\left(-\frac{\mu_n L_1}{a_1}\right)J_1\left(\frac{b_2}{a_1}\xi_n\right)}{\mu_n \sinh\left(\frac{\mu_n L_1}{a_1}\right)\xi_n J_0^2(\xi_n)} , \quad ka_1 < \xi_n$$

$$C_n = \frac{-2u_2\left(\frac{b_2}{a_1}\right)J_1\left(\frac{b_2}{a_2}\xi_n\right)}{\eta_n \sin\left(\frac{\eta_n L_2}{a_2}\right)\xi_n J_0^2(\xi_n)} , \quad ka_2 \geq \xi_n$$

$$C_n = \frac{2u_2\left(\frac{b_2}{a_1}\right)J_1\left(\frac{b_2}{a_2}\xi_n\right)}{\eta_n \sinh\left(\frac{\eta_n L_2}{a_2}\right)\xi_n J_0^2(\xi_n)} , \quad ka_2 < \xi_n .$$

In all of the above expressions, appropriate limiting values must be used when n = 1, since $\xi_1 = 0$.

DISTRIBUTION

DGRA/CS(RN)/DNOS	1
DAUWE/DUWP	2
Maritime Group DES(W)	3
CS(R)2e (Navy)	4
DPT17	5
Vickers Shipbuilding & Engineering Ltd (NAVED) (Attn Mr J Hackett)	6
DRIC	7 - 28
AMTE(T) file	29 - 40